Article

TRANSPARENT
PROCESS

THE
EMBO
JOURNAL

Role of glutamine and interlinked asparagine metabolism in vessel formation

Hongling Huang[1,2], Saar Vandekeere[1,2], Joanna Kalucka[1,2], Laura Bierhansl[1,2], Annalisa Zecchin[1,2], Ulrike Brüning[1,2], Asjad Visnagri[3], Nadira Yuldasheva[3], Jermaine Goveia[1,2], Bert Cruys[1,2], Katleen Brepoels[1,2], Sabine Wyns[1,2], Stephen Rayport[4,5], Bart Ghesquière[1,2], Stefan Vinckier[1,2], Luc Schoonjans[1,2], Richard Cubbon[3], Mieke Dewerchin[1,2], Guy Eelen[1,2,†] ⓘ & Peter Carmeliet[1,2,*,†] ⓘ

Abstract

Endothelial cell (EC) metabolism is emerging as a regulator of angiogenesis, but the precise role of glutamine metabolism in ECs is unknown. Here, we show that depriving ECs of glutamine or inhibiting glutaminase 1 (GLS1) caused vessel sprouting defects due to impaired proliferation and migration, and reduced pathological ocular angiogenesis. Inhibition of glutamine metabolism in ECs did not cause energy distress, but impaired tricarboxylic acid (TCA) cycle anaplerosis, macromolecule production, and redox homeostasis. Only the combination of TCA cycle replenishment plus asparagine supplementation restored the metabolic aberrations and proliferation defect caused by glutamine deprivation. Mechanistically, glutamine provided nitrogen for asparagine synthesis to sustain cellular homeostasis. While ECs can take up asparagine, silencing asparagine synthetase (ASNS, which converts glutamine-derived nitrogen and aspartate to asparagine) impaired EC sprouting even in the presence of glutamine and asparagine. Asparagine further proved crucial in glutamine-deprived ECs to restore protein synthesis, suppress ER stress, and reactivate mTOR signaling. These findings reveal a novel link between endothelial glutamine and asparagine metabolism in vessel sprouting.

See also: **B Kim et al** (August 2017) and **J Andrade & M Potente** (August 2017)

Introduction

Recent studies documented an important role of EC glycolysis and fatty acid oxidation in angiogenesis (De Bock et al, 2013a,b; Schoors et al, 2014, 2015), and illustrated that targeting endothelial cell (EC) metabolism may represent a novel anti-angiogenic strategy (Eelen et al, 2015). In contrast to the well-established role of glutamine metabolism in cancer cells (DeBerardinis & Cheng, 2010; Wise & Thompson, 2010), little is known about a possible role of glutamine metabolism in ECs during vessel sprouting. In fact, only a few previous papers reported enzyme kinetics of glutaminase 1 (GLS1), the enzyme metabolizing glutamine to glutamate, in EC homogenates and lysates (Leighton et al, 1987; Wu et al, 2000), or reported a role of GLS1 in preventing EC senescence (Unterluggauer et al, 2008). However, nothing is known about a role of glutamine metabolism in vessel formation *in vivo*, or in underlying processes of endothelial tip *versus* stalk cell specification. Endothelial tip cells are located at the forefront (tip) of the vascular sprout and lead the sprout by migrating (they do not/rarely proliferate) toward the source of angiogenic signals, which are sensed by protruding filopodia (Geudens & Gerhardt, 2011; Potente et al, 2011). Endothelial stalk cells following the tip cell elongate the vessel sprout through proliferation (Geudens & Gerhardt, 2011; Potente et al, 2011). Tip and stalk cell phenotypes are not pre-determined irreversible cell differentiation states, but rather can dynamically interchange, so that the EC with the greatest tip cell competitiveness always leads the vessel sprout at the tip (Jakobsson et al, 2010). Emerging evidence reveals that endothelial tip and stalk cells have characteristic metabolic signatures (De Bock et al, 2013b; Schoors et al, 2015). Given that glutamine is the most abundant non-essential amino acid (DeBerardinis & Cheng, 2010) and critical for many other cell types (Zhang et al, 2017), we hypothesized that glutamine metabolism might also be critical for vessel sprouting.

Glutamine is a key carbon/nitrogen source and is metabolized for ATP generation and macromolecule production in cancer cells

1 Laboratory of Angiogenesis and Vascular Metabolism, Department of Oncology, KU Leuven, Leuven, Belgium
2 Laboratory of Angiogenesis and Vascular Metabolism, Center for Cancer Biology, VIB, Leuven, Belgium
3 Leeds Institute of Cardiovascular & Metabolic Medicine, The University of Leeds, Leeds, UK
4 Department of Psychiatry, Columbia University, New York, NY, USA
5 Department of Molecular Therapeutics, New York State Psychiatric Institute, New York, NY, USA
*Corresponding author. Tel: +32 16 32 30 39; Fax: +32 16 37 25 85; E-mail: peter.carmeliet@kuleuven.vib.be
†Co-corresponding senior authors

(DeBerardinis & Cheng, 2010). Glutamine is first hydrolyzed by glutaminase (GLS) to ammonia and glutamate, which is then further metabolized to α-ketoglutarate (α-KG) via glutamate dehydrogenase (GLUD1) (Son *et al*, 2013). Glutamine is also used for the production of nucleotides and proteins (DeBerardinis *et al*, 2007), glutathione (GSH) for redox balance, and for the synthesis of the pro-angiogenic factors nitric oxide (NO) and polyamines. While glutamine donates its amino group at the gamma position for nucleotide synthesis (thereby being converted to glutamate), glutamate donates nitrogen at the alpha position for the synthesis of other non-essential amino acids in transamination reactions that convert glutamate to α-keto-glutarate (α-KG). Cell type-specific use of glutamine has been reported (DeBerardinis *et al*, 2007; Son *et al*, 2013; Mashimo *et al*, 2014). For instance, pancreatic ductal adenocarcinoma cells, but not other cancer cell types, rely on glutamine metabolism to maintain cellular redox homeostasis (Son *et al*, 2013). Several phase I clinical trials are ongoing to evaluate the safety, pharmacokinetics, and pharmacodynamics of the GLS1-specific inhibitor CB-839 in patients with hematological malignancies and solid tumors such as breast cancer, renal cancer, and lung cancer (www.clinicaltrials.gov). Whether and how ECs rely on glutamine metabolism is unknown.

Glutamine is also involved in mTORC1 activation and the ER stress response. mTORC1 is a master regulator of cell metabolism, controlling the synthesis of protein, lipids (Laplante & Sabatini, 2009), and nucleotides (Ben-Sahra *et al*, 2013). mTORC1 activity is stimulated by growth factors and amino acids (Jewell *et al*, 2013). In parallel with mTORC1, the ER stress response pathway can also sense nutrient deficiency. Amino acid deprivation can activate the serine threonine kinase GCN2 (general control nonderepressible 2), which in turn phosphorylates the translation initiation factor eIF2a, resulting in increased translation of the transcription factor activating transcription factor 4 (ATF4), which induces expression of multiple ER stress response genes (Harding *et al*, 2003). Several of these genes are involved in amino acid synthesis or transport, such as asparagine synthetase (ASNS), which catalyzes glutamine-dependent asparagine synthesis from aspartate (Harding *et al*, 2003).

The conditionally essential amino acid asparagine can be *de novo* synthesized by ASNS in most cells. In normal conditions, its expression levels are low, but they can be rapidly induced in response to limitation of glucose, asparagine, but also leucine, isoleucine or glutamine, or even a single essential amino acid, as may occur during protein limitation or an imbalanced dietary amino acid composition (Jousse *et al*, 2004; Balasubramanian *et al*, 2013). Low serum asparagine levels have also been documented in certain cancers (Scioscia *et al*, 1998), child stunting due to malnutrition (Semba *et al*, 2016), food deprivation (Ahlman *et al*, 1994), or dietary asparagine starvation (Newburg *et al*, 1975). In cancer cells, increased ASNS expression is a component of solid tumor adaptation to nutrient deprivation and/or hypoxia (Balasubramanian *et al*, 2013). Not a single report documented the expression or role of ASNS in ECs.

Serum asparagine levels are also therapeutically lowered to nearly undetectable levels as part of the treatment of various hematological cancers. Indeed, acute lymphoblastic leukemia (ALL) cells and some types of non-Hodgkin's lymphoma, including natural killer (NK)-cell lymphoma, are unable to produce sufficient asparagine for their growth, and therefore rely on the availability of extracellular asparagine (Kawedia & Rytting, 2014). This makes these cancer cells

sensitive to low asparagine levels, as can be therapeutically achieved by treatment with asparaginase, the enzyme that converts asparagine into aspartate and ammonia (Pieters *et al*, 2011; Chan *et al*, 2014). Delivering asparaginase to the bloodstream rapidly depletes plasma asparagine, causing a rapid efflux of cellular asparagine, which is then also metabolized, and thus, the cells of the entire body are challenged with asparagine depletion (Richards & Kilberg, 2006). Since asparagine is a downstream metabolite of glutamine, combined inhibition of GLS1 with asparagine deprivation is synthetically lethal for solid tumor cells (Li *et al*, 2017). Notably, asparaginase treatment is also effective for solid tumors, when combined with inhibition of autophagy (Zhang *et al*, 2016; Li *et al*, 2017).

Recent studies uncovered an important role of asparagine in cancer cell proliferation (Krall *et al*, 2016) and cell adaption to glutamine withdrawal (Zhang *et al*, 2014). It is also noteworthy that a defective ASNS gene blocks cells at the G1 step of the cell cycle (Gong & Basilico, 1990) and asparagine deprivation induces apoptosis (Aslanian *et al*, 2001). It has been postulated that asparagine limitation causes these effects, not simply through decreased availability for (glyco)protein synthesis, but possibly by serving another role, perhaps as a signal molecule. Since a link between glutamine and asparagine metabolism in ECs during vessel sprouting has not been studied, we characterized glutamine metabolism in ECs and provide proof-of-principle for blocking glutamine metabolism as a novel possible anti-angiogenic strategy.

Results

Glutamine metabolism is essential for endothelial cell sprouting *in vitro*

For an unbiased assessment of amino acid consumption/secretion, we cultured human umbilical vein endothelial cells (HUVECs, further abbreviated as "ECs") in standard M199 medium plus 20% fetal bovine serum (FBS) (concentrations of the different amino acids in this medium at the start of the experiment are listed in Fig EV1A). Subsequent measurements of consumption/secretion rates of various amino acids in the culture medium revealed that proliferating ECs consumed glutamine more than any other amino acid (Fig 1A). Given the dearth of published data on glutamine metabolism in ECs, we first characterized the consequences of glutamine deprivation (now utilizing glutamine-free M199 medium with dialyzed FBS to obtain zero glutamine levels). Notably, in the absence of glutamine, ECs failed to sprout (Fig 1B–E), and glutamine deprivation dose-dependently reduced EC proliferation (Fig 1F) and impaired migration (Fig 1G). In agreement, compared to quiescent ECs, glutamine uptake and oxidation were higher in proliferating ECs (Fig 1H and I).

In order to analyze the role of glutamine metabolism selectively in an EC-autonomous manner during angiogenesis *in vivo*, we generated and phenotyped mice lacking the rate-controlling glutaminase-1 (GLS1) in ECs (see below), realizing that GLS1 gene inactivation differs from glutamine starvation. However, we first characterized *in vitro* the effect of blocking/silencing GLS1 on EC behavior. Given the very low expression levels of GLS2 in ECs (Fig EV1B), we focused on GLS1. We silenced GLS1 expression by lentiviral transduction with a shRNA against GLS1 (GLS1[KD]), which lowered GLS1 expression by more than 75% (Fig EV1C and D).
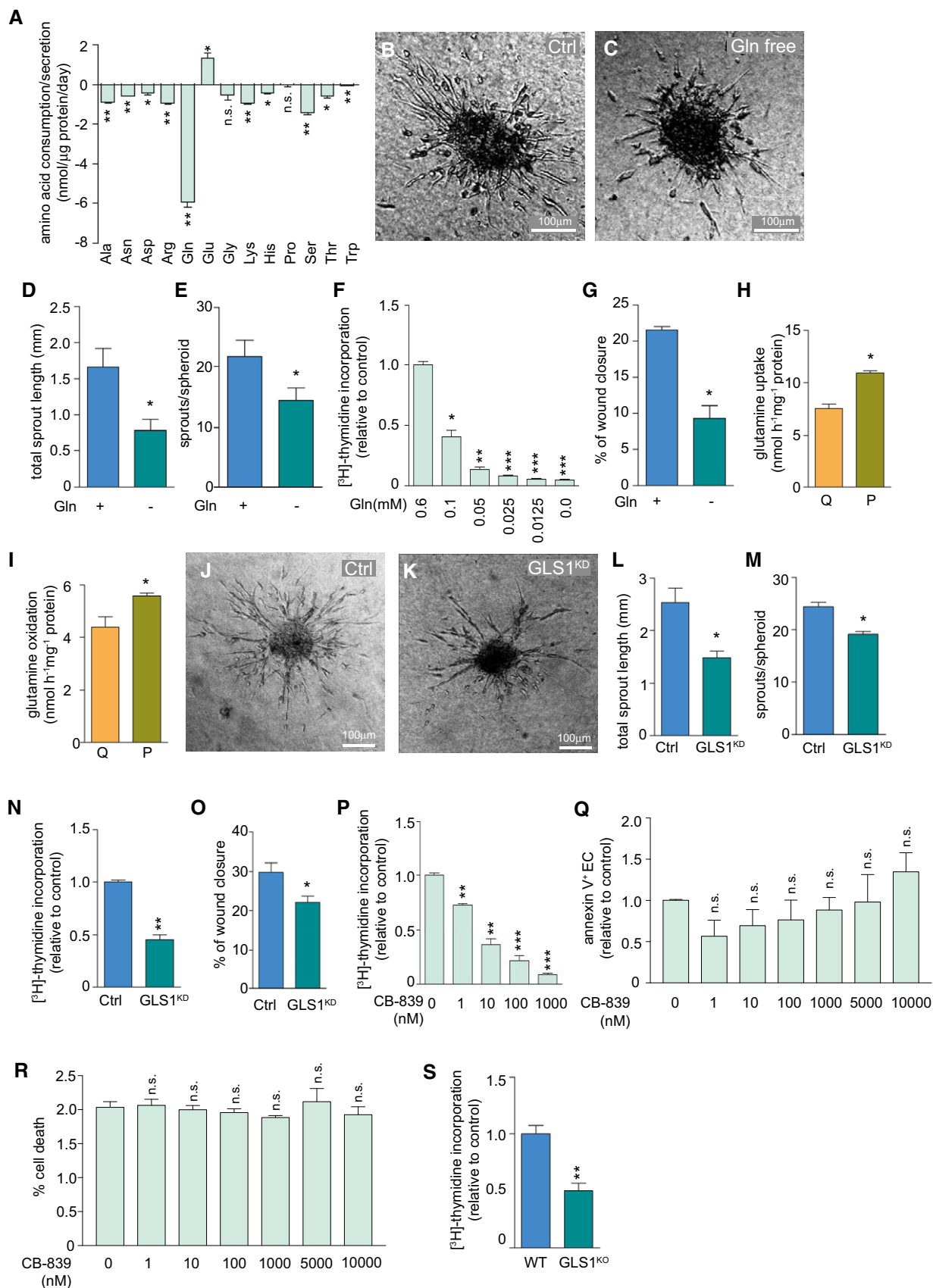
Figure 1.

◄

Figure 1. Glutamine metabolism sustains EC proliferation.

A   Quantification of amino acid consumption or secretion rate (values below zero indicate consumption, values above zero indicate secretion).

B–E   Representative images of EC spheroids sprouting under control (B) and glutamine-free conditions (C), and corresponding quantification of total sprout length (D) and number of sprouts per spheroid (E).

F $[^3H]$-Thymidine incorporation in DNA in ECs at different doses of extracellular glutamine.

G   Percentage of wound closure in control and glutamine-deprived ECs in monolayer scratch migration assays.

H, I   Quantification of glutamine uptake (H) and glutamine oxidation (I) in quiescent (Q) versus proliferating (P) ECs.

J–M   Representative images of control (J) and GLS1^{KD} (K) EC spheroids, and quantification of total sprout length (L) and number of sprouts per spheroid (M).

N $[^3H]$-Thymidine incorporation in DNA in control and GLS1^{KD} ECs.

O   Percentage of wound closure in control and GLS1^{KD} ECs in scratch migration assays.

P $[^3H]$-Thymidine incorporation into DNA in ECs treated with increasing concentrations of the GLS1 inhibitor CB-839.

Q   Annexin V$^+$ ECs (relative to control) after treatment with different concentrations of CB-839.

R   Percent cell death (measured by LDH release) in ECs treated with different concentrations of CB-839.

S $[^3H]$-Thymidine incorporation in DNA in mouse liver ECs isolated from GLS1^{ECKO} mice and their corresponding wild-type littermates (n = 3 for both genotypes).

Data information: All data are mean ± SEM from at least three independent experiments, each performed with ECs derived from a different individual donor. *P < 0.05, **P < 0.01, ***P < 0.001, n.s., not significant versus corresponding control (two-tailed unpaired t-test). For panel (A), a one-sample t-test versus a hypothetical value of 0 was used. Ala, alanine; Asn, asparagine; Asp, aspartate; Arg, arginine; Gln, glutamine; Glu, glutamate; Gly, glycine; Lys, lysine; His, histidine; Pro, proline; Ser, serine; Thr, threonine; Trp, tryptophan; Q, quiescent; P, proliferating; WT, wild type. Scale bars in (B, C, J and K) are 100 μm.

GLS1 knockdown (GLS1^{KD}) impaired EC sprouting (Fig 1J–M), proliferation (Fig 1N), and migration (Fig 1O). Treatment of ECs with the GLS1-specific blocker CB-839 (Gross *et al*, 2014) dose-dependently reduced EC proliferation (Fig 1P). Of note, CB-839 did not affect EC proliferation upon overexpression of GLS2, indicating that it did not inhibit GLS2 (Fig EV1E). Also, supplementation of exogenous glutamate (the end-product of the GLS reaction) over-ruled the anti-proliferative effect of CB-839, confirming that this blocker selectively inhibited GLS1 (Fig EV1F). Interestingly, blocking GLS1 activity did not induce apoptosis (Figs 1Q and EV1G and H) or cytotoxicity (Fig 1R), arguing against a general cell demise as underlying cause for the above effects on EC behavior.

For confirmation, we isolated mouse endothelial cells (mECs) from the liver of GLS1^{ECKO} mice, which were generated by inter-crossing GLS1$^{lox/lox}$ mice (Mingote *et al*, 2015) with Pdgfb-Cre^{ERT2} mice (an EC-specific Cre-driver line) (Claxton *et al*, 2008). Prior to mEC isolation, GLS1 was deleted from the endothelium by five consecutive days of tamoxifen treatment. GLS1 mRNA expression levels were substantially reduced in GLS1^{KO} mECs (Fig EV1I), which proliferated less actively (Fig 1S), confirming the data obtained with GLS1 silencing and pharmacological blockade.

Glutamine metabolism is essential for vessel sprouting *in vivo*

In order to examine the role of endothelial glutamine metabolism *in vivo*, we analyzed vascular development in GLS1^{ECKO} mice, using the postnatal retinal angiogenesis model (Stahl *et al*, 2010). Isolectin-B4 (IB4) staining of retinal vessels of GLS1^{ECKO} pups at postnatal day 5 (P5) revealed that endothelial loss of GLS1 diminished the number of vascular branch points both at the front and the rear of the vascular plexus (Fig 2A–D) and reduced radial expansion of the plexus (Fig 2E). Confirming the above *in vitro* data, endothelial loss of GLS1 reduced EC proliferation as revealed by counting ECs, stained for IB4 and phospho-histone 3 (phH3) (Fig 2F–H). Fewer distal sprouts with filopodia were observed in GLS1^{ECKO} pups, suggestive of an EC migration defect (Fig 2I). In addition, loss of GLS1 in ECs did not affect vessel maturation, determined by NG2 staining for mural cell pericyte coverage (Fig 2J–L).

We also explored if pharmacological blockade of glutamine metabolism reduced pathological angiogenesis and therefore used the

oxygen-induced model of retinopathy of prematurity (ROP). In this model, mouse pups are exposed to hyperoxia during postnatal days P7–P12. This causes capillary depletion and vascular rarefaction, which induces retinal ischemia upon return to ambient oxygen levels, and secondary formation of proliferative vascular tufts between P12 and P17 (Scott & Fruttiger, 2010). Treatment of pups with the GLS1 blocker CB-839 from P12 to P17 reduced the formation of vascular tufts at P17 (Fig 2M–O). These findings underscore the importance of endothelial GLS1-driven glutamine metabolism in both developmental and pathological angiogenesis. However, given that we only studied retinal angiogenesis models, analysis of angiogenesis in other organs is warranted in the future.

Glutamine metabolism regulates tip/stalk cell specification

To substantiate the finding that blocking GLS1 inhibits vessel sprouting and to obtain further underlying mechanistic insight, we studied EC tip cell competition, given the key role of tip/stalk cell dynamics in sprouting angiogenesis (Jakobsson *et al*, 2010; De Bock *et al*, 2013b). Since this requires a chimeric EC spheroid approach, whereby glutamine metabolism is inhibited in half of the ECs, we used a mix of ECs, in which GLS1 was silenced or which were trans-duced with a control shRNA. Using such chimeric spheroids consist-ing of a 1/1 ratio of mCherry$^+$-control (red) and GFP$^+$-GLS1^{KD} (green) ECs, we observed that GLS1^{KD} ECs displayed reduced competitiveness to obtain the tip position in the spheroid sprout (Fig 2P–R). These data argue for a prominent role for GLS1 in tip/stalk cell dynamics, revealing that glutamine metabolism is essential for ECs to reach the tip position in the vessel sprout.

Glutamine metabolism is redundant for other vascular functions

In order to assess whether GLS1 selectively regulated vessel formation, we also explored if glutamine metabolism by GLS1 affected other features of the endothelium, such as vascular tone, EC activation (in the context of vascular inflammation), and EC differentiation (arterial, venous, lymphatic). However, blocking GLS1 did not affect the expression levels of endothelial nitric oxide synthase (eNOS) or endothelin 1 (ET-1), key regulators of vascular tone (Forstermann & Sessa, 2012; Liu *et al*, 2003; Fig 2S). Likewise,
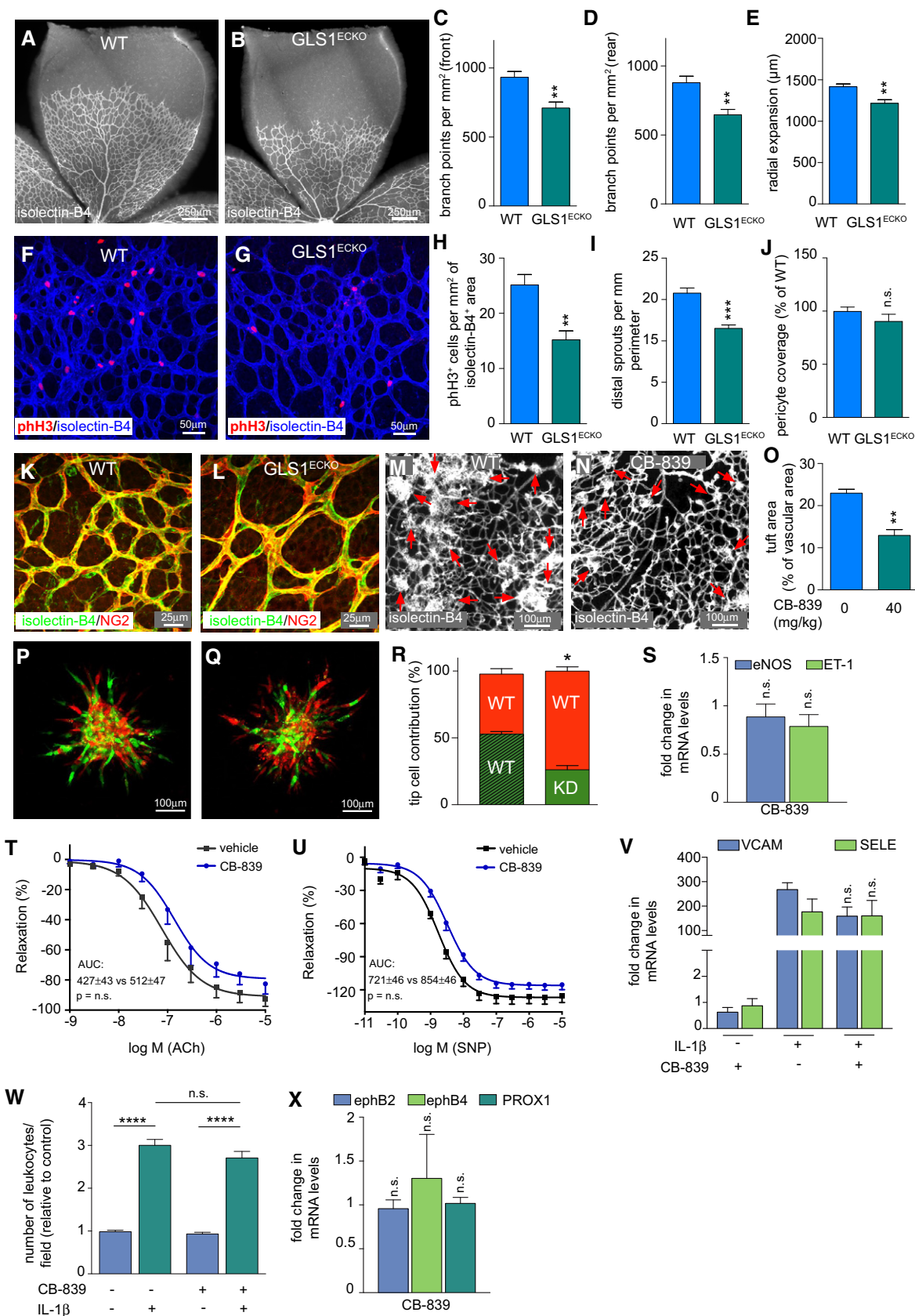
Figure 2.

Figure 2. GLS1 inhibition causes sprouting defects in retinal angiogenesis.

A, B   Representative pictures from isolectin-B4 (IB4)-stained retinal vascular plexus obtained from wild-type (A) or GLS1[ECKO] (B) mice at P5.

C–E   Quantification of branch points at the front (C) or rear (D), and radial expansion (E) of the retinal vascular plexus in wild-type and GLS1[ECKO] animals ($n = 9$).

F, G   Representative pictures of IB4/phospho-histone 3 (phH3) double-stained wild-type (F) and GLS1[ECKO] (G) retinal vasculature at P5.

H   Quantification of phH3[+] ECs in the retinal vascular plexus of wild-type and GLS1[ECKO] mice ($n = 6$).

I   Quantification of distal sprouts with filopodia in the retinal vasculature of wild-type and GLS1[ECKO] mice at P5 ($n = 7$).

J–L   Quantification of pericyte coverage (NG2^{+}/IB4^{+} area in % of wild-type) ($n = 6$) (J), and corresponding representative pictures of IB4/NG2 (pericyte marker) double staining of P5 wild-type (K) and GLS1[ECKO] (L) retinal vascular plexus.

M–O   Representative images of retinal flat mounts of retinopathy of prematurity (ROP) mice treated with vehicle (M) or CB-839 (N) (red arrows indicate vascular tufts) and corresponding quantification of vascular tuft area (O) ($n = 8$).

P–R   Representative pictures of mosaic spheroids consisting of a 1:1 mixture of mCherry[+]-control (red) and GFP[+]-control (green) ECs (P) or a 1:1 mixture of mCherry[+]-control (red) and GFP[+]-GLS1[KD] (green) ECs (Q) and quantification (per spheroid) of percentages of red versus green ECs occupying the tip cell position (R) ($n = 3$).

S   Fold changes in mRNA level of eNOS and endothelin-1 in CB-839-treated ECs ($n = 4$).

T, U   Relaxation of aortic rings pretreated with vehicle or CB-839 in response to acetylcholine (T) and in response to the nitric oxide donor sodium nitroprusside (U) ($n = 8$).

V   Fold changes in mRNA levels of VCAM and E-selectin in CB-839-treated ECs under IL-1β stimulation ($n = 4$).

W   Quantification of number of leukocytes adhering to a vehicle- or CB-839-treated EC monolayer under IL-1β stimulation ($n = 4$).

X   Fold changes in mRNA level of arterial (ephrin B2), venous (ephrin B4), and lymphatic (Prox1) markers in CB-839-treated ECs ($n = 4$).

Data information: All data are mean ± SEM; n refers to the number of individual animals per genotype or per treatment group, or to the number of individual EC donors used, or to the number of aortic rings analyzed. **$P < 0.01$, ***$P < 0.001$, ****$P < 0.0001$, n.s., not significant versus corresponding control (two-tailed unpaired t-test). Panels (S, V, X) represent data as fold change versus control with a value equal to 1 meaning no change in mRNA level for a given condition in comparison with the control condition. In panels (S, X), statistical differences indicate if the fold change differs from 1. In panel (V), statistical differences are calculated versus the control IL-1β-treated condition. An area under the curve (AUC) analysis was used in panels (T, U). ACh, acetylcholine; eNOS, endothelial nitric oxide synthase, ephB2; ephrin B2; ephB4, ephrin B4; ET-1, endothelin 1; IL-1β, interleukin 1β; phH3, phospho-histone 3; PROX1, prospero homeobox 1; NG2, chondroitin sulfate proteoglycan 4; SELE, selectin-E; SNP, sodium nitroprusside; VCAM, vascular cell adhesion molecule; WT, wild type. Scale bars are as follows: 250 μm in (A, B); 50 μm in (F, G); 25 μm in (K, L), and 100 μm in (M, N, P, Q).

ex vivo treatment of aortic rings with CB-839 did not affect vasorelaxation (Fig 2T and U). Second, we assessed the expression of the adhesion molecules VCAM and E-selectin upon IL-1β stimulation in order to explore whether glutamine metabolism affected the activation of the endothelium in conditions of vascular inflammation (Kalucka *et al*, 2017). GLS1 inhibition did, however, not alter the expression of these markers (Fig 2V) or the adhesion of leukocytes (Fig 2W). Finally, we checked the effect of GLS1 inhibition on arterial, venous, and lymphatic specification. No effect was seen on the expression of ephrin B2 (arterial marker), ephrin B4 (venous marker), and Prox1 (lymphatic marker) (dela Paz & D'Amore, 2009; Kume, 2010; Fig 2X). Taken together, GLS1 inhibition affected tip cell competitiveness in vessel sprouting, yet had no effect on other key features of the endothelium.

Glutamine controls multiple metabolic functions in ECs

To explore how glutamine metabolism regulates EC sprouting, we studied various possible mechanisms, using glutamine starvation as experimental approach.

Anaplerosis & energy homeostasis

(i) Glutamine is an anaplerotic carbon source for the TCA cycle in cancer cells (Wise & Thompson, 2010). However, since glutamine can be used in a cell type-specific manner, and ECs have a different metabolism than cancer cells and other cell types (Schoors *et al*, 2015), we explored whether ECs used glutamine for anaplerosis. [U-13C]-glutamine tracing in ECs revealed that glutamine donated carbons to several TCA cycle intermediates, often even more than [U-13C]-glucose (Fig 3A). Not surprisingly therefore, glutamine deprivation depleted the intracellular pool of TCA metabolites (Fig 3B). (ii) Glutamine metabolism was, however, largely dispensable for ATP production in ECs, as glutamine deprivation did not alter intracellular ATP levels (Fig 3C) or the energy charge, defined as ([ATP] + 1/2 [ADP])/([ATP] + [ADP] + [AMP]) (Fig 3D). Thus,

glutamine deprivation did not cause an energy crisis, likely because ECs generate most of their energy via glycolysis (De Bock *et al*, 2013b).

Amino acid synthesis

We analyzed the intracellular levels of non-essential amino acids (NEAAs), because glutamine is a precursor of several NEAAs. Glutamine starvation lowered the intracellular pool of glutamate (Glu), aspartate (Asp), and asparagine (Asn), while not affecting (or even slightly increasing) the levels of alanine (Ala), serine (Ser) and glycine (Gly) (Fig 3E). Consistently, [U-13C]-glutamine and [15N2]-glutamine tracing experiments showed high label incorporation into glutamate, aspartate, and asparagine, but much less (minimally) in alanine, serine, and glycine (Fig 3F).

Macromolecule synthesis

We examined the effect of glutamine deprivation on macromolecule synthesis, in particular of proteins, nucleotides, and lipids. (i) Protein synthesis: consistent with the fact that glutamine itself and glutamine-derived NEAAs are used as building blocks for proteins, glutamine starvation reduced protein synthesis in ECs (Fig 3G). (ii) Nucleotide synthesis: [15N2]-glutamine tracing showed that glutamine donated its nitrogen for nucleotide synthesis in ECs under glutamine-replete conditions (Fig EV2A). In agreement, glutamine starvation lowered the intracellular pool of deoxynucleotides (dNTPs; Fig EV2B), consistent with the proliferation defect. Glutamine starvation did, however, not affect the intracellular pool of ribonucleotides (rNTPs; Fig EV2C), possibly due to an increased activity of salvage pathways or lower net rNTP consumption. (iii) Lipid synthesis: we explored if glutamine contributes to lipogenesis in ECs through reductive carboxylation (Metallo *et al*, 2012; Mullen *et al*, 2012), but found only marginal label incorporation in M + 5 citrate upon [U-13C]-glutamine incubation (Fig EV2D). In cells with high malic enzyme activity, glutamine-derived pyruvate can also serve as a lipogenic substrate (Metallo *et al*, 2012). However, in
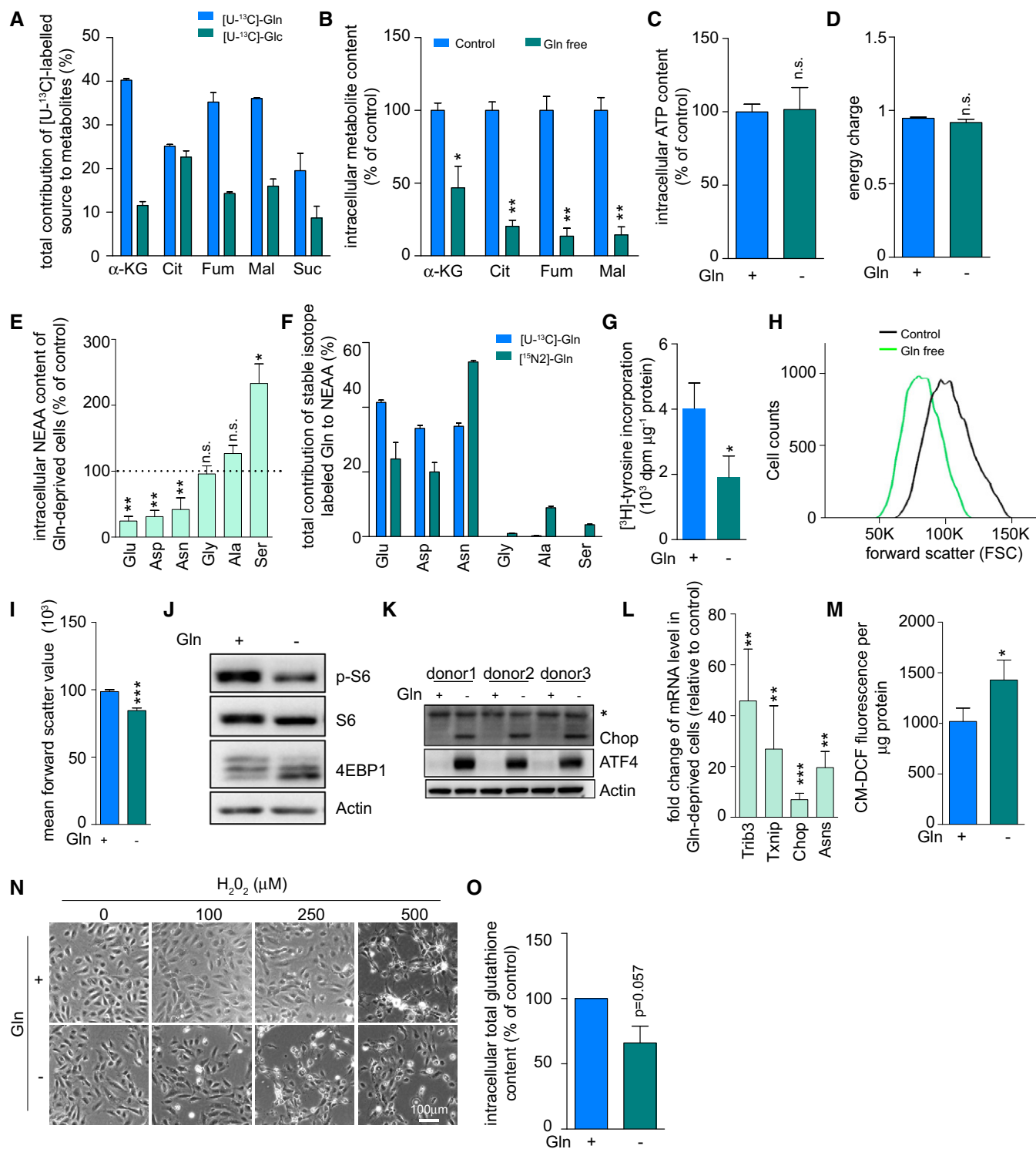
Figure 3.

[U-^{13}C]-glutamine labeled ECs, glutamine-derived carbons in pyruvate and lactate were nearly undetectable (Fig EV2D). In agreement, compared to [U-^{14}C]-labeled glucose and acetate, label incorporation from [U-^{14}C]-glutamine into the lipid fraction was much lower (Fig EV2E). Although a driving force for glutamine-mediated lipogenesis in cancer cells (Metallo *et al*, 2012; Schug *et al*, 2015),

hypoxia did not increase the incorporation of [U-^{14}C]-glutamine-derived carbon into the lipid fraction in ECs (Fig EV2F).

mTOR signaling

Glutamine modulates mTOR signaling (Duran *et al*, 2012; Jewell *et al*, 2015) and endoplasmic reticulum (ER) stress (Zhang *et al*,

Figure 3.   Glutamine controls multiple metabolic functions in ECs.

A   Gas chromatography–mass spectrometry (GC-MS)-based analysis of total contribution of [U-^{13}C]-glutamine and [U-^{13}C]-glucose to tricarboxylic acid (TCA) intermediates in ECs. [U-^{13}C]-Glutamine and [U-^{13}C]-glucose were supplemented to the culture medium at 2 and 5.5 mM final concentration, respectively. All labelings were performed under steady-state conditions.

B   Quantification of intracellular TCA metabolites in control and glutamine-deprived (Gln free) ECs.

C   Intracellular ATP levels measured by liquid chromatography–mass spectrometry (LC-MS) in control and glutamine-depleted ECs.

D   Energy charge measurement in control and glutamine-deprived ECs.

E   Intracellular levels of the non-essential amino acids glutamate, aspartate, asparagine, alanine, glycine, and serine in control and glutamine-deprived ECs. Level in control cells is indicated by the dashed line.

F   Total contribution of [U-^{13}C]-glutamine carbon and [^{15}N2]-glutamine nitrogen to non-essential amino acids in ECs.

G   Measurement of protein synthesis rate ([^{3}H]-tyrosine incorporation) in control and glutamine-deprived ECs.

H, I   Representative cell size distribution graph (H) and corresponding quantification of cell sizes (I) measured by forward scatter value of flow cytometry in control and glutamine-deprived ECs.

J   mTOR signaling activity in control and glutamine-deprived ECs, revealed by immunoblotting for phosphorylated ribosomal protein S6 (p-S6) and by 4EBP1 mobility shift. β-Actin was used as loading control. Representative blot of three independent experiments is shown.

K   Measurement of ER stress in control and glutamine-deprived ECs, determined by accumulation of ATF4 and Chop protein. β-actin was used as a loading control. Results from three independent experiments are shown. Asterisk indicates a non-specific band.

L   mRNA levels of ER stress marker genes in glutamine-deprived versus control ECs determined by qRT–PCR.

M   Intracellular reactive oxygen species (ROS) levels in control and glutamine-deprived ECs measured by CM-DCF staining.

N   Representative pictures of control and glutamine-deprived ECs at 2 h after treatment with increasing concentrations of H$_2$O$_2$. In glutamine starvation (but not control) conditions, treatment with 250 μM H$_2$O$_2$ already resulted in cell death, revealed by loss of normal cell morphology.

O   Total glutathione content in control and glutamine-deprived ECs.

Data information: All data are mean ± SEM of at least three independent experiments each performed with ECs from a different individual donor. *$P < 0.05$, **$P < 0.01$, ***$P < 0.001$, n.s., not significant versus corresponding control (two-tailed unpaired *t*-test). α-KG, α-ketoglutarate; Cit, citrate; Fum, fumarate; Mal, malate; Suc, succinate; NEAA, non-essential amino acids; Chop, C/EBP homologous protein; ATF4, activating transcription factor 4; Trib3, Tribbles Pseudokinase 3; Txnip, thioredoxin-interacting protein; Asns, asparagine synthetase; CM-DCF, 5-(and-6)-chloromethyl-2′,7′-dichlorodihydrofluorescein diacetate. Scale bar in (N) is 100 μm.

2014). In agreement, glutamine starvation reduced the size of ECs (Fig 3H–I), and decreased mTOR activity (Fig 3J). The ER can also sense amino acid deficiencies, and trigger an ER stress response (Parsa *et al*, 2007). In agreement with previous studies (Qie *et al*, 2012), we observed that glutamine starvation induced the expression of C/EBP homologous protein (Chop) and ATF4 (Fig 3K) and of several other ER stress marker genes, such as asparagine synthetase (ASNS), thioredoxin-interacting protein (Txnip), and tribbles pseudokinase 3 (Trib3) (Fig 3L).

Redox homeostasis

We also examined if glutamine is critical for redox homeostasis. Glutamine deprivation impairs proliferation, in part by elevating intracellular ROS levels (Son *et al*, 2013). In agreement, intracellular ROS levels were elevated in glutamine-deprived ECs (Fig 3M). Moreover, glutamine-starved ECs were more sensitive to ROS-induced cell death (Fig 3N). In agreement, glutamine-depleted ECs showed a trend toward reduced total glutathione levels (Fig 3O).

Asparagine supplementation and TCA cycle fueling restore proliferation of glutamine-deprived ECs

We then explored, using an unbiased approach, how we could rescue the EC proliferation defect induced by glutamine deprivation. Supplementing dNTPs or a nucleoside mixture failed to restore proliferation of glutamine-deprived ECs (Fig EV3A). Replenishing the TCA cycle by adding extra carbons with cell-permeable dimethyl-α-ketoglutarate (DM-α-KG, further abbreviated to α-KG for readability), monomethyl-succinate (MM-succinate, further abbreviated to suc), oxaloacetate (OAA), or pyruvate recovered EC proliferation for only 20–25% (Fig EV3B). A similar modest rescue was achieved by supplementing glutamine-starved cells with a pool of

NEAAs (Fig EV3C). Supplementation of the antioxidant N-acetylcysteine (NAC) or the cell-permeable glutathione ethyl ester (GSH-EE) also failed to recover EC proliferation upon glutamine depletion (Fig EV3D and E).

The above results show that restoring individual parameters of the glutamine deprivation-induced cellular alterations was insufficient to yield a complete rescue. We therefore tested combination strategies. Surprisingly, the combination of α-KG plus NEAAs was able to fully rescue the proliferation defect of glutamine-deprived ECs (Fig 4A). Further sub-analysis revealed that asparagine was the only NEAA critically needed for a full rescue, when given in combination with α-KG (Fig 4B). In agreement with the proliferation rescue, the α-KG plus asparagine combination was able to restore intracellular dNTP pools (Fig 4C). In fact, as long as asparagine was provided, all other carbon sources capable of TCA replenishment (pyruvate, OAA, MM-succinate) were able to largely restore proliferation of glutamine-deprived ECs (Fig EV3F). The combination of asparagine plus α-KG also rescued all other glutamine-dependent phenotypes, including the intracellular pool of the TCA intermediates (Fig 4D), cell size (Fig 4E–F), mTORC1 signaling (Fig 4G), protein synthesis (Fig 4H), the ER stress response (Fig 4I), and redox imbalance (Fig 4J and K). These data underscore the importance of asparagine and TCA replenishment in rescuing the metabolic and cellular changes of glutamine-starved ECs.

Asparagine alone partially rescues glutamine-restricted EC defects

We then studied the role of asparagine in rescuing the proliferation defect of glutamine-deprived ECs in more detail. In total absence of glutamine, supplementation of asparagine alone was unable to rescue the proliferation defect (Fig 4B and L). However, in low
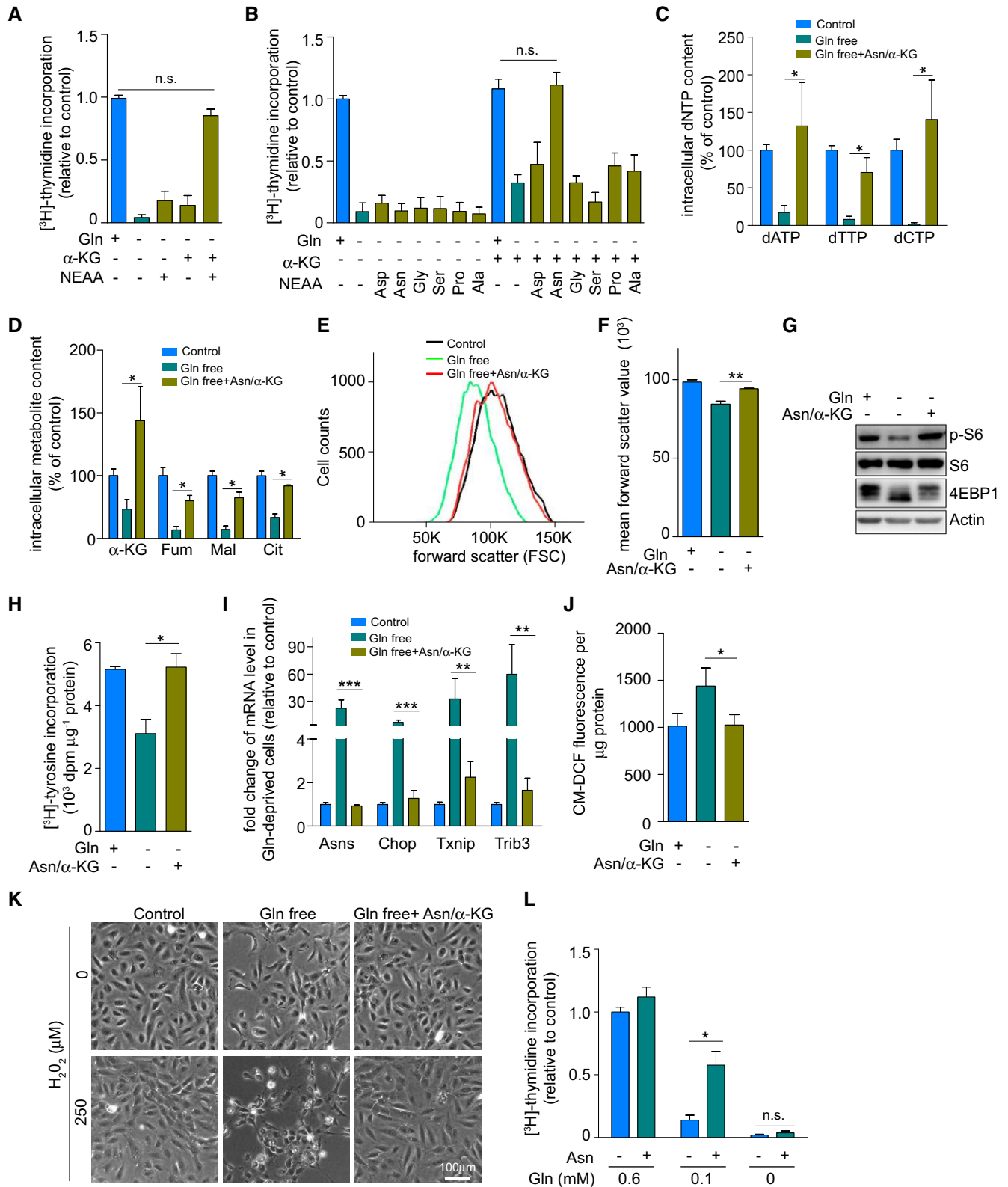
Figure 4.

glutamine conditions (0.1 mM), supplementation of asparagine alone was capable of partially restoring EC proliferation (Fig 4L). These data further emphasize the pivotal role of asparagine in

glutamine metabolism-restricted ECs and suggest that maintaining cellular asparagine levels in ECs is necessary to ensure cellular homeostasis.

Figure 4. Asparagine and TCA anaplerosis are required for EC proliferation under glutamine-depleted conditions.

A   [³H]-Thymidine incorporation in DNA in glutamine-starved ECs with and without supplementation of exogenous cell-permeable dimethyl α-ketoglutarate (hereafter referred to as α-KG) or a non-essential amino acid mixture (NEAA).

B   [³H]-Thymidine incorporation in DNA in glutamine-starved ECs with and without single or combined supplementation of exogenous α-KG and individual NEAAs.

C   Quantification of intracellular deoxynucleotide (dNTP) levels in control and glutamine-free (without or with supplementation of asparagine and α-KG) conditions.

D   Quantification of intracellular TCA metabolites in control or glutamine-deprived ECs with and without combined supplementation of asparagine and α-KG.

E, F   Representative graph of cell size distribution (E) determined by flow cytometry and corresponding quantification of cell size (F) of control or glutamine-deprived ECs with and without combined supplementation of asparagine and α-KG. Of note, the first two bars in this graph are the same as in Fig 3I. The data in the two panels originate from the same set of experiments, only in panel (F) an additional condition is displayed.

G   mTOR activation, revealed by immunoblotting for phosphorylated ribosomal protein S6 (p-S6) and by 4EBP1 mobility shift, in control or glutamine-deprived ECs with and without combined supplementation of asparagine and α-KG. β-Actin was used as loading control. Immunoblots shown are representative of three independent experiments.

H   Protein synthesis ([³H]-tyrosine incorporation assay) in control and glutamine-deprived ECs with and without combined supplementation of asparagine and α-KG.

I   mRNA levels of ER stress markers in control or glutamine-deprived ECs with and without combined supplementation of asparagine and α-KG.

J   Intracellular reactive oxygen species (ROS) levels (CM-DCF staining) in control and glutamine-deprived ECs with and without combined supplementation of asparagine and α-KG.

K   Representative pictures of control and glutamine-deprived ECs with and without combined supplementation of asparagine and α-KG at baseline and at 2 h after treatment with H_2O_2.

L   [³H]-Thymidine incorporation into DNA in ECs grown at different concentrations of glutamine, with or without supplementation of asparagine.

Data information: All data are mean ± SEM from at least three independent experiments each performed with ECs from a different individual donor. *$P < 0.05$, **$P < 0.01$, ***$P < 0.001$, n.s., not significant versus corresponding control (two-tailed unpaired *t*-test). Pro, proline; dATP, deoxyadenosine triphosphate; dTTP, deoxythymidine triphosphate; dCTP, deoxycytidine triphosphate; all other abbreviations as in previous figures. Scale bar in (K) is 100 μm.

ECs use glutamine to synthesize asparagine

The above data indicate that asparagine (in combination with some TCA cycle anaplerosis) is critical to rescue the cellular defects of glutamine-deprived ECs, while glutamine deprivation lowered the levels of asparagine (Fig 3E). This connection between glutamine and asparagine raised the question whether ECs need to maintain asparagine levels for proliferation and cellular homeostasis, and whether glutamine is necessary for asparagine production. We therefore hypothesized that ECs, in glutamine-replete conditions, might *de novo* synthesize asparagine, a reaction catalyzed by asparagine synthetase (ASNS; Richards & Kilberg, 2006), an enzyme that uses glutamine as nitrogen donor to convert aspartate into asparagine. These experiments were performed in culture medium containing 100 μM asparagine (unlike M199 medium, 20% FBS contains asparagine), that is, within the range of physiological asparagine plasma levels in adults (50–130 μM) (Armstrong & Stave, 1973; Scriver *et al*, 1985). ECs indeed expressed detectable levels of ASNS, especially in conditions of hypoxia or ER stress (Figs 5A and EV3G), consistent with previous reports in other cell types (Pan *et al*, 2003; Cui *et al*, 2007; Ameri *et al*, 2010). Tracing studies further revealed a high contribution (54%) of [¹⁵N2]-glutamine into asparagine (Fig 3F), confirming that glutamine was used for asparagine synthesis by ASNS in ECs. Furthermore, ASNS^KD, lowering its expression by 73% (Figs 5A and EV3H) in the presence of glutamine reduced EC proliferation and impaired vessel sprouting (Fig 5B–F).

We then used medium without asparagine to explore whether re-addition of extracellular asparagine could rescue the proliferation defects induced by impaired asparagine synthesis in ASNS^KD ECs. Indeed, supplementation of extracellular asparagine rescued the proliferation defect induced by ASNS^KD (Fig 5F), thus showing the importance of asparagine, regardless of whether it is *de novo* synthesized or taken up from the extracellular milieu. These data support the notion that under glutamine-replete conditions, proliferating ECs rely on *de novo* asparagine synthesis or asparagine uptake.

Multiple mechanisms of the asparagine-mediated rescue

In an attempt to explore how asparagine rescued the EC defects in glutamine-deprived conditions, we studied different reported biological functions of this amino acid. (i) Consistent with the fact that asparagine is used for protein synthesis (Ubuka & Meister, 1971), we noted that asparagine supplementation recovered protein synthesis in glutamine-deprived ECs (Fig 5G). (ii) Asparagine is also known to be essential for the adaptation of cancer cells to glutamine deprivation by suppressing the ER stress response (Zhang *et al*, 2014). Consistent with this, supplying asparagine to glutamine-deprived ECs mitigated the ER stress response (Fig 5H). (iii) Asparagine was recently identified as mTOR complex 1 (mTORC1) regulator by virtue of its role as an amino acid exchange factor (Krall *et al*, 2016). Interestingly, supplying asparagine (but not α-KG) indeed reactivated mTOR signaling in glutamine-deprived ECs (Fig 5I). In summary, while unraveling the role of glutamine metabolism in ECs, we unexpectedly found a pivotal role for glutamine-dependent asparagine and its synthesis in vessel sprouting.

Discussion

This study provides the following key novelties: (i) It demonstrates for the first time the role and importance of glutamine metabolism for angiogenesis *in vitro* and (using GLS1^ECKO mice) *in vivo*. (ii) It unravels a critical role of glutamine as both carbon and nitrogen donor to sustain EC growth. (iii) It identifies a new mechanism in ECs of how glutamine affects vessel growth, that is, through a previously unknown reliance on asparagine, which ECs can *de novo* synthesize by asparagine synthetase (ASNS) or take up from the extracellular milieu; this study also documents for the first time evidence for a key role of ASNS in vessel sprouting. (iv) It uncovers biological functions of asparagine in ECs, that is, for protein synthesis, mTOR activation and suppression of glutamine deprivation-induced ER stress. And, finally, (v) it provides unprecedented
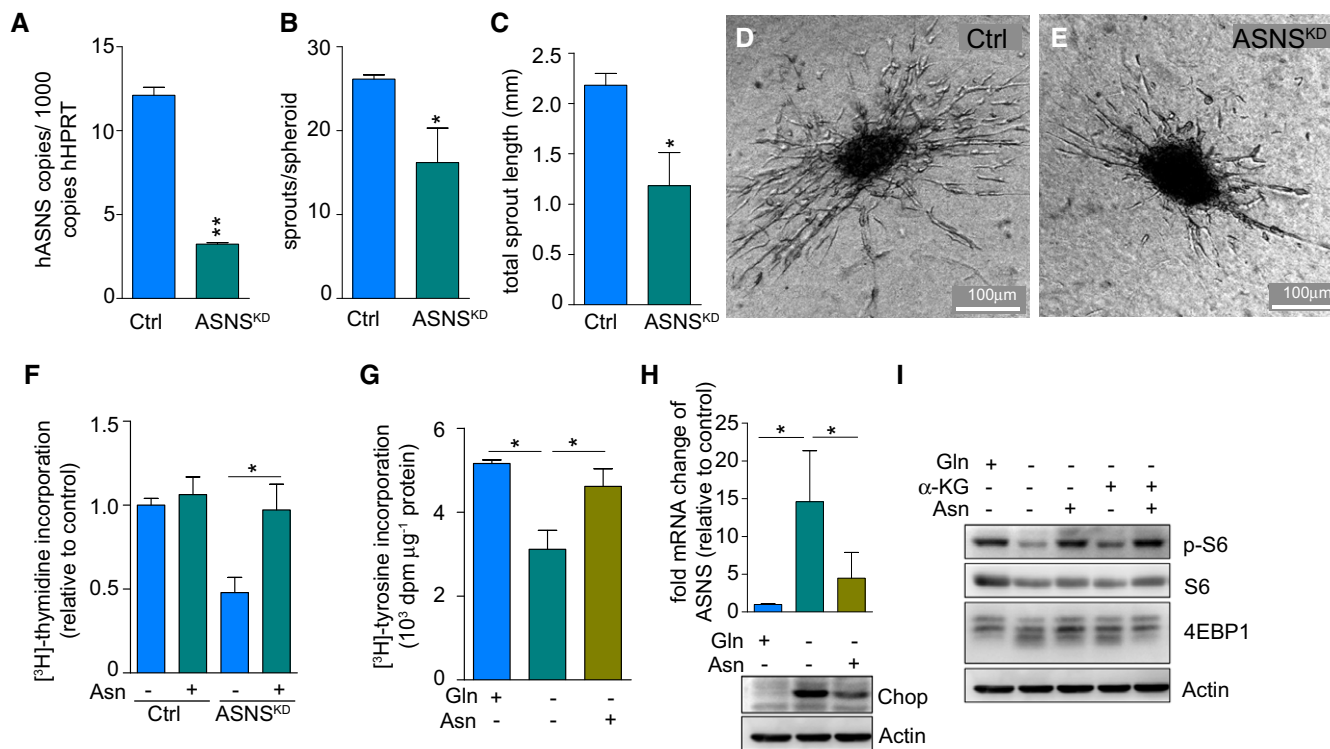
Figure 5. Glutamine-dependent asparagine synthesis is required for vessel sprouting.

A   mRNA level of ASNS in control and ASNS^{KD} ECs.

B–E   Quantification of number of sprouts (B) and total sprout length (C) in control and ASNS^{KD} EC spheroids and corresponding representative images (D, E).

F   [^{3}H]-Thymidine incorporation into DNA in control and ASNS^{KD} ECs with or without asparagine supplementation.

G   Protein synthesis ([^{3}H]-tyrosine incorporation assay) in control and glutamine-deprived ECs with and without supplementation of asparagine. Of note, the first two bars in this graph are the same as in Fig 4H. The data in the two panels originate from the same set of experiments, only in panel (G) another third condition is displayed.

H   mRNA and protein levels of ER stress markers in control and glutamine-deprived ECs with and without supplementation of asparagine.

I   Representative immunoblots of mTOR activation, revealed by immunoblotting for phosphorylated ribosomal protein S6 (p-S6) and 4EBP1 mobility shift, in control and glutamine-deprived ECs with and without single or combined supplementation of asparagine and α-KG. Of note, the first three lanes of the β-actin loading control are the same as the β-actin loading controls in panel (H) because the Chop immunoblotting was done in the same experiment but was found to fit more logically in panel (H).

Data information: All data are mean ± SEM from at least three independent experiments each performed with ECs from a different individual donor. *$P < 0.05$, **$P < 0.01$, n.s., not significant versus corresponding control (two-tailed unpaired *t*-test). ASNS, asparagine synthetase; other abbreviations as in previous figures. Scale bar in (D, E) is 100 μm.

evidence that pharmacological blockade of GLS1 inhibits pathological angiogenesis as a potential novel anti-angiogenic strategy, and identifies ASNS as a potential novel target for therapeutic angiogenesis inhibition.

Glutamine regulates angiogenesis via multiple mechanisms

Earlier studies documented the expression of glutaminolysis genes in ECs (Leighton *et al*, 1987; Lohmann *et al*, 1999), but did not evaluate the role of glutamine metabolism in vessel sprouting *in vivo*. Here, we show that glutamine is indispensable for vessel sprouting both *in vitro* and in mouse models of developmental and pathological angiogenesis *in vivo*. Like many cancer cells (Hosios *et al*, 2016), ECs too consume high amounts of extracellular glutamine, and in fact consume more glutamine than any other amino acid. Glutamine metabolism is crucial for ECs, since glutamine deprivation severely impaired EC proliferation and vessel sprouting. Of note, during final revision of our manuscript we became aware of another study under

consideration at this same journal reporting complementary findings on the role of glutamine metabolism in ECs during angiogenesis (Kim *et al*, 2017). This adds further value to our findings on the crucial role for glutamine metabolism in vessel sprouting.

Mechanistically, lack of glutamine caused multiple types of cellular defects, including reduced protein synthesis, decreased TCA anaplerosis, redox imbalance, and inactivation of mTOR signaling. Together, these defects suffice to explain the impaired angiogenesis upon glutamine deprivation *in vitro* or following genetic inhibition or pharmacological blockade of GLS1 *in vivo*. Glutamine has been previously implicated in several of these mechanisms in other cell types (mostly malignant cells; DeBerardinis & Cheng, 2010), though never in ECs. When considering these mechanisms, ECs thus seemingly resemble cancer cells.

However, in sharp contrast to cancer cells, for which single treatments like replenishment of the TCA cycle (van den Heuvel *et al*, 2012) or supplementation of antioxidants (Son *et al*, 2013) sufficed to rescue the phenotypes, these and other single treatments failed to

rescue glutamine deprivation-induced proliferation arrest in ECs. Possibly, the genetic instability of cancer cells (Tardito *et al*, 2015) might perhaps enable them to cope more flexibly with glutamine deprivation-induced cellular changes. The stronger reliance of ECs on glutamine on the other hand might create an opportunity for selective targeting of ECs in the tumor microenvironment.

Notably, glutamine metabolism was dispensable for energy homeostasis, as glutamine starvation did not affect ATP levels or the energy charge. This should, however, not be surprising, as ECs rely primarily on glycolysis to generate > 85% of their ATP (De Bock *et al*, 2013b).

Interestingly, chimeric EC spheroid assays revealed that GLS1 promoted tip cell competitiveness. This is likely attributable to the role of GLS1 in EC migration, as high motility is essential for ECs to reach the tip position in the vascular sprout (Bentley *et al*, 2009; Jakobsson *et al*, 2010). While the precise mechanisms of how glutamine metabolism regulates EC motility remain to be defined, circumstantial evidence provides a link to cellular migration. Indeed, glutamine metabolism regulates migration of non-EC types (Kim *et al*, 2014), promotes cancer cell migration and dissemination by altering signaling pathways (Han *et al*, 2013, 2017; Rodrigues *et al*, 2016), is essential for the tip cell motility machinery (Sakai *et al*, 2015), and regulates adhesion receptors (Hou *et al*, 2014). Furthermore, through regulating redox homeostasis, glutamine metabolism might also affect cell migration (Parri & Chiarugi, 2013; Son *et al*, 2013). Of note, glutamine metabolism was less/not important for other endothelial functions, such as regulation of vascular tone, inflammation, or differentiation.

Glutamine-dependent angiogenesis—novel link to asparagine

The combination treatment of asparagine with an anaplerotic carbon donor rescued the defects of glutamine-deprived ECs. Under low glutamine conditions, asparagine mono-treatment could even partially rescue the EC defects, implying that maintaining asparagine levels is crucial for ECs to sustain growth and homeostasis. The finding that asparagine can rescue glutamine-low phenotypes suggests that asparagine is downstream of glutamine's activity in ECs. Indeed, isotope tracing experiments showed that glutamine-derived carbon and nitrogen are incorporated into asparagine in ECs. To maintain asparagine levels, ECs can rely on endogenous *de novo* synthesis by ASNS, or alternatively, they can take up extracellular asparagine. Hence, ECs are equipped with mechanisms to take up asparagine when available, or to synthesize it themselves in nutrient-limited environments, such as can occur when ECs migrate into avascular regions to vascularize tissues, or when present in the tumor setting.

Endothelial cells may additionally rely on ASNS in conditions when ASNS expression levels are elevated (upon glucose or amino acid deprivation, hypoxia, or ER stress) or when asparagine levels in the extracellular milieu are low (in certain cancers, or upon protein limitation, unbalanced amino acid intake, asparaginase treatment, etc.; Newburg *et al*, 1975; Burt *et al*, 1983; Ahlman *et al*, 1994; Scioscia *et al*, 1998; Suliman *et al*, 2005; Tong *et al*, 2014; Semba *et al*, 2016). In fact, asparaginase treatment of neonatal pups, which depleted asparagine without affecting glutamine levels in the blood (Fig EV4A), did not impair retinal angiogenesis (Fig EV4B–F), suggesting that endothelial ASNS provided the

necessary asparagine to mediate glutamine's role in angiogenesis, though formal confirmation would require analysis of angiogenesis in mice lacking ASNS in ECs. These findings provide the first evidence for a role of ASNS and asparagine downstream of glutamine metabolism in angiogenesis.

Asparagine—coordinating EC homeostasis with metabolic reserves?

Mechanistically, upon glutamine deprivation, asparagine treatment restored protein synthesis, suppressed the ER stress response, and reactivated mTOR signaling. Of note, when cancer cells use asparagine to exchange amino acids for mTOR activation, they have a net asparagine efflux (Krall *et al*, 2016). However, the finding that ECs consumed asparagine and thus lowered asparagine levels in the culture medium suggests that ECs did not activate mTOR signaling via this exchange mechanism.

Emerging evidence in cancer and transformed cells indicates that intracellular asparagine has a more important role than previously expected in regulating cell survival in response to glutamine withdrawal, as recently illustrated by a study using glioblastoma cancer cells (Zhang *et al*, 2014), but it remained unknown whether this is also the case for healthy non-transformed cells. In neuroblastomas, ASNS levels correlated with c-Myc amplification and are the highest in dedifferentiated brain cancer cells, when progressing from adenoma to carcinoma (Zhang *et al*, 2014). Given that: (i) cancer cells rewire their metabolism differently than healthy non-transformed cell types; (ii) the cancer cell genotype is mutated (unlike healthy non-transformed cells) which may rewire metabolism differently; and (iii) EC metabolism differs from that of cancer and immune cells (Schoors *et al*, 2015), metabolic concepts in cancer cells cannot be simply extrapolated to normal healthy cells in general, or to ECs in particular. In addition, glutamine depletion of glioblastoma cells increased apoptosis, and asparagine suppressed the glutamine deprivation-induced apoptosis, but not the proliferation defect upon glutamine withdrawal (Zhang *et al*, 2014). In contrast, we show that in ECs asparagine plus α-KG rescue the proliferation defect and all other glutamine-dependent phenotypes, including the intracellular pool of the TCA intermediates, cell size, mTORC1 signaling, protein synthesis, the ER stress response, and redox imbalance. Healthy ECs thus fundamentally differ from transformed cancer cells in their response to glutamine starvation and their usage of asparagine in mediating this response.

Even though a role for asparagine has been traditionally confined to protein synthesis alone (unlike the other 19 common amino acids; Ubuka & Meister, 1971), increasing evidence suggests alternative roles for this amino acid as a metabolite that coordinates cellular homeostatic responses with metabolic fuel reserves and availability. Since intracellular asparagine levels are the lowest of all non-essential amino acids in proliferating cells (Zhang *et al*, 2014), and asparagine amination exclusively relies on glutamine, asparagine synthesis has been proposed to be a rheostat, sensing the availability of TCA cycle intermediates and the supply of reduced nitrogen to maintain non-essential amino acid synthesis (Zhang *et al*, 2014). Hence, carbohydrate and amino acid starvation may trigger asparagine biosynthesis, because asparagine is an indicator of insufficient substrate for continued cell division. This notion is further supported by findings in glioblastoma cells that other amino

acid synthesis pathways are not as highly regulated and other amino acids do not appear to play as critical a role (Zhang *et al*, 2014). In addition, reduced intracellular asparagine levels have been shown to induce ATF4-dependent signaling (Zhang *et al*, 2014), implying that this metabolite can serve as a signaling metabolite. Also of note, it has been proposed that because the carbon to nitrogen ratio of asparagine is less than that for glutamine, plants switch to asparagine as the primary nitrogen transporter and storage molecule to spare carbon during carbohydrate starvation (Kilberg & Barbosa-Tessmann, 2002). Whether mammalian ECs can also rely on asparagine for these purposes, or utilize this amino acid as a signaling metabolite, are exciting but outstanding questions that require further study.

Possible therapeutic implications

Even though future research is warranted to assess effects on angiogenesis in other organs, pharmacological blockade of GLS1 reduced pathological ocular angiogenesis, suggesting an alternative therapeutic strategy for diseases caused by excess vessel growth. Furthermore, the different enzymes involved in the asparagine-glutamine interplay can potentially represent novel anti-angiogenic targets. As such, our *in vitro* data show how silencing ASNS inhibits EC sprouting. In this respect, inhibiting intracellular asparagine production by blocking ASNS in ECs in combination with depleting extracellular asparagine levels (by asparaginase treatment) may offer novel therapeutic opportunities for anti-angiogenesis in pathological conditions, as was suggested for cancer cells (Zhang *et al*, 2014). This might be attractive for inhibiting tumor angiogenesis, given that an increasing number of studies document that asparaginase treatment, in combination with GLS1 or autophagy inhibition, is also effective in slowing down solid tumor growth. Hence, blocking GLS1 or ASNS merit further attention as alternative strategies to inhibit pathological angiogenesis.

Materials and Methods

Chemicals and reagents

Collagen type 1 (rat tail) and nucleoside mix (100 X) were from Merck-Millipore. The GLS1 inhibitor CB-839 was kindly provided by Calithera BioSciences (South San Francisco, CA, USA). dNTP mix, all amino acids, pyruvate, oxaloacetate, glutathione reduced ethyl ester, dimethyl-α-ketoglutarate (DM-α-KG, this is the cell-permeable form, which was used for supplementation/rescue experiments and which we further abbreviated to α-KG in the text and figures for reasons of readability), monomethyl-succinate (MM-Succinate), thapsigargin, tamoxifen, and asparaginase were purchased from Sigma-Aldrich. Non-Essential Amino Acids Solution (NEAA, 100X) was from ThermoFisher Scientific. [^{3}H]-Thymidine, [^{3}H]-tyrosine, [U-^{14}C]-L-glutamine, [U-^{14}C]-acetate, and [U-^{14}C]-L-glucose were from Perkin Elmer. [U-^{13}C]-L-glutamine, [U-^{13}C]-D-glucose, and [^{15}N2]-L-glutamine were purchased from Cambridge Isotope Laboratories.

The following primary antibodies or dyes were used: isolectin Griffonia simplicifolia (GS)-IB4-Alexa 488, isolectin GS-IB4-Alexa 568, isolectin GS-IB4-Alexa 647 (Molecular Probes), anti-phH3

(Merck-Millipore), anti-NG2 (AB5320; Chemicon), anti-4EBP1 (9452), anti-p-S6 (S235/236), anti-S6, anti-Chop (2895), anti-ATF4 (11815), anti-caspase-3 (9662) (Cell Signaling Technology), anti-β-actin, secondary Alexa-488, Alexa-568, or Alexa-633 conjugated antibodies were from Molecular Probes.

Cell culture

Freshly isolated (protocol as described previously; Jaffe *et al*, 1973) human umbilical vein endothelial cells (ECs) were cultured in M199 medium (Invitrogen) containing 20% FBS, 1 mg/ml D-glucose, heparin, 100 U/ml penicillin, 100 µg/ml streptomycin, and endothelial cell growth factor supplements (ECGS; 30 mg/l). As specified below under "Glutamine deprivation assay and rescue", a specific set of experiments required the use of glutamine-free M199 supplemented with 20% dialyzed serum. The ECs were isolated and used with approval of the Medical ethical commission of KU Leuven/University hospital Leuven (file S57123), and with informed consent obtained from all subjects. ECs were regularly tested for mycoplasma and only used between passages 1 and 5. ECs were kept at 37°C and 5% CO$_2$, and the growth medium was changed at least every other day. Hypoxia incubation of ECs was at 1% oxygen for 18 h, and thapsigargin treatment was at 1 µM for 18 h. When needed, ECs were grown to quiescence following a previously established model of contact inhibition (De Bock *et al*, 2013b). In brief, ECs were seeded at an initial density of 15,000 cells/cm^2 and were allowed to grow to a fully contact-inhibited, quiescent monolayer for 6–7 days with regular medium changes. To obtain a corresponding proliferative control, contact-inhibited cells (at day 6) were trypsinized and cultured in growth medium for at least 36 h to re-initiate proliferation. HEK293T cells (ATCC) were grown in DMEM, supplemented with 10% fetal bovine serum (FBS), 100 U/ml penicillin, and 100 µg/ml streptomycin. For stimulation with an inflammatory cue, ECs were treated with IL-1β (1 ng/ml, ThermoFisher, 10139HNAE25) for 2 h (37°C, 5% CO$_2$) prior to downstream experiments. Mouse liver endothelial cells (mECs) were isolated from healthy livers of 8- to 10-week-old control or GLS1^{ECKO} mice. Prior to isolation, GLS1^{ECKO} mice (see further below) and their control littermates were treated with tamoxifen (30 mg/kg) for 5 consecutive days to delete GLS1 from the endothelium. Mice were anesthetized with Nembutal (60 mg/kg) and were then perfused with 5 ml of a water-based perfusion buffer containing 1.7 M NaCl, 84 mM KCl, 120 mM HEPES, and 1 mM NaOH followed by 5 ml of a PBS-based digestion buffer containing 0.1% collagenase II, collagenase I, 2 mM CaCl$_2$, 1% antibiotic-antimycotic (Thermo Fisher Scientific) and 10% FBS (Biochrome) at a perfusion rate of 1 ml/min. Perfusion was considered complete when the liver and mesenteric vessels were blanched and the desired amount of digestion buffer (≥ 5 ml) had passed through the circulatory system. Livers were dissected, placed into a 50-ml conical tube with 3 ml of digestion buffer and incubated at 37°C for approximately 30 min, with regular shaking. After digestion, the tissue was homogeneously dissociated and the reaction was stopped with 10 ml of isolation buffer containing PBS plus 0.1% BSA (Sigma-Aldrich). Subsequently, the cell suspension was filtered through a 100 µm cell strainer and cells were washed twice with isolation buffer. Finally, the ECs were isolated by magnetic bead sorting with Dynabeads (CELLection™ Biotin Binder

Kit, Thermo Fisher Scientific) coated with anti-mouse CD31 (eBioscience, Anti-Mouse CD31 Clone 390), according to the manufacturer's instructions. Cells recovered from bead isolation were resuspended in M199 medium and plated at the desired density on cell culture plates pre-coated with 0.1% gelatin.

Knockdown and overexpression strategies

Lentiviral overexpression constructs for GLS2 were created by cloning the cDNA into pRRLsinPPT.CMV.MCS MM WPRE vector (Michieli *et al*, 2004). shRNA vectors against GLS1 (TRCN0000051135, TRCN0000051136; yielding similar results) and ASNS (TRCN0000290113, TRCN0000290105; yielding similar results) were purchased from Sigma. Lentiviruses were produced by transfecting 293T cells as previously described (Carlotti *et al*, 2004). A nonsense scrambled shRNA sequence was used as a negative control. Cells were transduced overnight at a multiplicity of infection (MOI) of 10, which was kept for all shRNA and overexpression experiments. Transduced cells were used in functional assays at least 3–4 days post-transduction.

RNA isolation and gene expression analysis

RNA was extracted from the lysate using the PureLink RNA Mini Kit (Ambion), according to the manufacturer's protocol. The concentration and purity of the extracted RNA was measured using the Nanodrop 2000 (Thermo Scientific). RNA samples were stored at −80°C or immediately converted to cDNA using the iScript cDNA Synthesis Kit (Bio-Rad), according to the manufacturer's instructions. An Applied Biosystems 7500 Fast device with in-house-designed primers and probes or premade primer sets (Applied Biosystems or Integrated DNA Technologies; sequences and/or primer set ID numbers available upon request) was used for quantitative RT–PCR analyses. Hypoxanthine-guanine phosphoribosyltransferase (HPRT) was used as a housekeeping gene. For comparison between GLS1 and GLS2, absolute expression levels were determined based on respective cDNA standard curves, and levels are expressed as copies mRNA per 10^3 copies HPRT mRNA.

Immunoblot analysis

Extraction of protein was performed in RIPA buffer (25 mM Tris–HCl (pH 7.6), 150 mM NaCl, 1% NP-40, 1% sodium deoxycholate, 0.1% SDS), supplemented with protease and phosphatase inhibitor mixes (Roche Applied Science), and followed by shearing genomic DNA. Lysates were then separated by SDS–PAGE under reducing conditions, transferred to a nitrocellulose or PVDF membrane, and analyzed by immunoblotting. Signal was detected using the ECL system (Amersham Biosciences, GE Healthcare) or SuperSignal Femto Western blotting substrate (Thermo Fisher Scientific) according to the manufacturer's instructions.

In vitro assays

Measurement of amino acid consumption or secretion rate
Cells were initially seeded in M199 full medium. After 24 h, cells were re-fed with fresh full medium (T0) and some of the T0 medium was kept for assessment of initial amino acid concentrations

(Fig EV1A). ECs were then allowed to grow for 48 h prior to medium sampling (T48). Medium from T0 and T48 was subjected to LC-MS analysis (see below), and the consumption or secretion rates were calculated accordingly. Please note that although there is no asparagine in M199 medium, supplementation of 20% normal FBS brings asparagine levels to around 100 μM. *[³H]-thymidine incorporation*: Proliferation was measured by incubating cells with 1 μCi/ml [³H]-thymidine for 2 h. Thereafter, cells were fixed with 100% ethanol for 15 min at 4°C, precipitated with 10% trichloroacetic acid (TCA) and lysed with 0.1 N NaOH. The amount of [³H]-thymidine incorporated into DNA was measured by scintillation counting and corrected for cell number. *[³H]-tyrosine incorporation*: To determine protein synthesis rate, cells were incubated with medium containing 1 μCi/ml [³H]-tyrosine for 6 h. Thereafter, medium was removed and cells were washed with ice-cold PBS. After protein precipitation with 10% TCA for more than 1 h, suspensions were transferred to an Eppendorf tube. Subsequently, the protein pellet was collected by a centrifugation at $21,000 \times g$ for 15 min. Finally, the protein pellet was dissolved in 0.5 M NaOH and 0.1% Triton X-100. The amount of [³H]-tyrosine incorporated into protein was measured by scintillation counting and corrected for protein content. *Spheroid sprouting assay*: ECs were incubated overnight in hanging drops in M199 medium containing 20% methylcellulose (Sigma-Aldrich) to form spheroids. Then, they were embedded in collagen gel as described (Korff *et al*, 2004) and cultured for 24 h to allow sprouting. Finally, spheroids were fixed with 4% PFA at room temperature and imaged under bright field using a Motic AE 31 microscope (Motic Electric Group Co Ltd.) or a Leica DMI6000B microscope (Leica Microsystems). Analysis of the number of sprouts per spheroid and the total sprout length (cumulative length of primary sprouts and branches per spheroid) was done on phase contrast images using the NIH ImageJ software package. *Mosaic spheroids for tip cell competition* were generated as indicated above, and consisted of a 1/1 mixture of GFP⁺-GLS1^KD ECs and mCherry⁺-wt ECs. Spheroids consisting of a 1/1 mixture of GFP⁺-wt ECs and mCherry⁺-wt ECs were used as controls in this setup. Tip cell competition was assessed by manual counting of the number of red versus green ECs at the tip of individual sprouts per spheroid. Control spheroids yielded a near 50/50% distribution at the tip position, indicating that overexpression of GFP versus mCherry by itself has no effect on tip cell competition. *Leukocyte adhesion assay*: Whole blood from healthy human volunteers was collected and anticoagulated with K₂EDTA (1.8 mg/ml, using plastic whole blood spray-coated K₂EDTA tubes, Becton Dickinson). Peripheral blood mononuclear cells (PBMCs) were isolated by gradient centrifugation over Ficoll-paque plus (GE Healthcare). PBMCs were labeled with Calcein (cell-permeant dye, ThermoFisher Scientific). ECs (plated 5 days before (7.5×10^4 cells/well, 12-well plate) to reach a confluent, contact-inhibited, quiescent monolayer) were washed with PBS and incubated either with vehicle (sterile PBS) or CB-839 (100 nM), overnight (37°C, 5% CO_2). After this period, medium was removed and ECs were washed with PBS. The mononuclear cells were added (5×10^5/well) and incubated for 60 min (37°C, 5% CO_2). Non-adherent cells were removed by washing five times with PBS, and cells were fixed using 4% PFA. Five fields per well, randomly chosen, were analyzed, and the number of adherent leukocytes per field was determined using a Leica DMI6000B microscope (magnification 20×). *Scratch wound*

migration assay: At T0, a scratch was made in confluent EC mono-layers using a sterile 200 µl pipette tip and cells were further incubated for 8 h (T8). Wound closure (gap area at T0 minus gap area at T8) was measured with NIH ImageJ software. *Glutamine deprivation assay and rescue*: Cells were initially seeded in full medium for 1 day. Cells were re-fed with glutamine-deprived medium (Thermo Fisher Scientific) with 20% dialyzed FBS (Thermo Fisher Scientific), 1 mg/ml D-glucose, heparin, 100 U/ml penicillin, 100 µg/ml strepto-mycin, and endothelial cell growth factor supplements (ECGS; 30 mg/l) for 24 h prior to the start of experiments. For all the rescue experiments, metabolites were added at the time of refeeding cells with glutamine-deprived medium; asparagine was added at 2 mM, DM-α-KG at 1 mM, NEAA mix at 1 mM (final concentration for each amino acid), individual NEAAs at 5 mM (some of the NEAAs required heating the medium to 37°C for optimal solubility and required readjustment of the pH after adding), pyruvate at 5 mM, mono-methyl hydrogen succinate at 5 mM, oxaloacetate at 4 mM, N-acetylcysteine at 10 mM, and glutathione reduced ethyl ester at 1 mM. Cell number counting was used as a measure of proliferation in glutamine-deprived cells when treated with dNTPs (500 µM) or nucleoside mix (10X); [^{3}H]-thymidine incorporation cannot be used as a measure for proliferation here as addition of dNTPs and NSX dilutes the [^{3}H]-thymidine pool. dNTPs and nucleoside mix were added at the same time as glutamine deprivation was initiated. The absolute cell number was counted every 24 h using a hemocyto-meter. *Bicinchoninic acid (BCA) assay (Pierce)* was used to determine protein content following manufacturer's guidelines. *Intracellular reactive oxygen species (ROS) detection*: 10 µM 5-(and-6)-chloro-methyl-2′,7′-dichlorodihydro fluorescein diacetate (CM-DCF) dye (Thermo Fisher Scientific) was added to cell culture medium for 30 min. After washing with PBS, cells were incubated in fresh culture medium for 30 min. Finally, CM-DCF fluorescence was measured with a plate reader and normalized to protein content. *Energy charge assessment:* 5×10^5 cells were collected in 100 µl ice-cold 0.4 M perchloric acid containing 0.5 mM EDTA. The protein pellet was removed by centrifugation at $21,000 \times g$ for 15 min. The pH of the supernatant was adjusted with 100 µl of 2 M K_2CO_3. 100 µl of the mixture was subsequently injected onto an Agilent 1260 HPLC with a C18-Symmetry column (150 × 4.6 mm; 5 mm; Waters), thermostated at 22.5°C. Flow rate was kept constant at 1 ml/min. A linear gradient using solvent A (50 mM NaH_2PO_4, 4 mM tetrabutylammonium, adjusted to pH 5.0 with H_2SO_4) and solvent B (50 mM NaH_2PO_4, 4 mM tetrabutylammonium, 30% CH_3CN, adjusted to pH 5.0 with H_2SO_4) was accomplished as follows: 95% A for 2 min, from 2 to 25 min linear increase to 100% B, from 25 to 27 min isocratic at 100% B, from 27 to 29 min linear gradient to 95% A, and finally from 29 to 35 min at 95% A. ATP, ADP, and AMP were detected at 259 nm. The energy charge is calculated as ([ATP] + 1/2 [ADP])/([ATP] + [ADP] + [AMP]). *Flow cytometry*: 5×10^5 cells were collected and resuspended in 500 µl PBS prior to analysis by flow cytometry (BD FACS Verse). To measure cell size, the voltages were adjusted to have the mean forward light scatter (FSC) of the control population at a value of 100,000. These voltages were kept constant for all samples. FlowJo analysis software (FlowJo, LLC) was used to determine the mean FSC value as a measure for cell size. *Annexin V/PI apoptosis measurement*: Cells were collected by trypsinization and resus-pended in binding buffer (10 mM HEPES, 140 mM NaCl, 2.5 M

$CaCl_2$ (pH = 7.4)). After counting, Annexin V antibody and PI were added at room temperature in the dark for 15 min prior to acquisi-tion on a BD FACS Aria. Data were analyzed with FlowJo analysis software. *LDH release assay (cytotoxicity)*: Cell death was measured by determining LDH release in the medium with the Cytotoxicity Detection Kit (Roche Applied Sciences) following manufacturer's instructions. *Nuclear DNA degradation*: Cells were seeded in 24-well plates and treated with the indicated doses of CB-839 for 24 h. Treatment with doxorubicin at 1 µg/ml (final concentration) for 24 h was used as a positive control. Then, cells were trypsinized, subjected to a centrifuge spin, and resuspended in PBS. From this suspension, aliquots were deposited on slides with a cytospin centri-fuge. For morphological analysis, cells were fixed with ice-cold methanol for 10 min and washed twice with PBS. Cells were then stained with TUNEL (Roche Therapeutics) according to the manu-facturer's conditions. Next, Hoechst 33258 (1/1,000 in PBS) was put on the cells for 10 min at room temperature and mounted with Pro-Long Gold. Nuclei were imaged on a Leica fluorescence microscope. *H_2O_2 challenge assay*: Cells were treated with the indicated concen-trations of H_2O_2 for 2 h. Bright field pictures were taken with a Leica DMI6000 microscope (Leica Microsystems, Mannheim, Germany). *Glutamine oxidation assay*: Glutamine oxidation was measured as $^{14}CO_2$ formation as previously described (De Bock *et al*, 2013b). In brief, cells were grown for 6 h in medium containing [U-^{14}C]-gluta-mine (0.5 µCi/ml) (Perkin Elmer). Perchloric acid ($HClO_4$) (2 M) was added to lyse the cells and to promote the release of CO_2. Immediately after adding perchloric acid, the wells were covered with a hyamine hydroxide-saturated Whatman filter paper. After overnight absorption at room temperature, the paper was trans-ferred to scintillation vials for liquid scintillation counting. *Gluta-mine uptake assay*: Cells were incubated with medium containing 0.5 µCi/ml [U-^{14}C]-L-glutamine for 30 min after which they were washed at least five times with ice-cold PBS. The last PBS wash was collected and checked for residual radioactivity. Cells were then lysed with 0.2 N NaOH, and lysates were used for scintillation counting. *^{14}C-glutamine, glucose, and acetate incorporation into lipid fraction*: Cells were incubated with medium containing 0.5 µCi/ml [U-^{14}C]-L-glutamine, 0.5 µCi/ml [U-^{14}C]-L-glucose, or 0.5 µCi/ml [U-^{14}C]-L-acetate for 24 h after which lipid fractions were prepared by a two-phase methanol–water–chloroform extraction method. In brief, cells were washed at least three times with ice-cold PBS followed by a protein precipitation step by adding 800 µl methanol: water (5:3) solution. Cells were scratched with a rubber policeman, and the lysates were transferred to fresh Eppendorf tubes; 500 µl chloroform was added subsequently. After vortexing, the mixture was centrifuged at $21,000 \times g$ for 15 min to form an upper polar phase and a lower non-polar (lipid) phase. The incorporation of ^{14}C-glucose, ^{14}C-glutamine, or ^{14}C-acetate into lipid fraction was calcu-lated as counts per minute (cpm) in non-polar fraction divided by cpm in whole cell extract. To compare the incorporation of gluta-mine carbon in normoxia versus hypoxia, a similar method was performed except that cells were cultured in 0.5% oxygen for 1 day during the phase of tracer incubation.

LC-MS analysis

For all stable isotope labeling experiments, cells were incubated for 48 h with labeled substrates in a 100% labeling way (glucose:

5.5 mM; glutamine: 2 mM). Metabolites from 5×10^5 cells were extracted in 150 μl methanol–acetonitrile–water (50:30:20) solution. Next, the extracts were centrifuged at 4°C for 15 min at 20,000 × *g* and the supernatants were used for LC-MS. Measurements were performed using a Dionex UltiMate 3000 LC System (Thermo Scientific) in-line connected to a Q-Exactive Orbitrap mass spectrometer (Thermo Scientific). 40 μl of sample was injected and loaded onto a SeQuant ZIC/pHILIC Polymeric column (Merck-Millipore). A linear gradient was carried out starting with 84% solvent A (95-5 acetonitrile-H$_2$O, 2 mM ammonium acetate pH 9.3) and 16% solvent B (2 mM ammonium acetate pH 9.3). From 2 to 29 min, the gradient changed to 75% B and was kept at 75% until 34 min. Next, a decrease to 16% B was carried out to 42 min, and then, 16% B was maintained until 58 min. The solvent was used at a flow rate of 100 μl/min, and the column temperature was kept constant at 25°C. The mass spectrometer operated in negative ion mode; settings of the HESI probe were as follows: sheath gas flow rate at 25, auxiliary gas flow rate at 5 (at a temperature of 260°C). Spray voltage was set at 4.8 kV, temperature of the capillary at 300°C, and S-lens RF level at 50. Normal full scan (resolution of 35,000 and scan range of m/z 50–1,050) was applied. In case of low metabolite levels (such as dNTPs), a targeted Selected Ion Monitoring (SIM) method was applied. Data collection (total metabolite abundances as well as ^{13}C or ^{15}N isotopic incorporation) was performed with the Xcalibur software (Thermo Scientific). For calculation of the total carbon/nitrogen contribution, we corrected for naturally occurring isotopes using the method of Fernandez *et al* (1996). For relative metabolite levels, the total ion count was normalized to the protein content. The total contribution of carbon/nitrogen was calculated using the following equation (Fendt *et al*, 2013):

$$\text{Total contribution of carbon/nitrogen} = \sum_{i=0}^{n} i \times m_i \bigg/ \left(n \sum_{i=0}^{n} m_i \right)$$

where *n* is the number of C or N atoms in the metabolite, *i* represents the different mass-isotopomers, and *m* refers to the abundance of a certain mass.

GC-MS analysis

For GC-MS analyses, 5×10^5 cells were extracted in 800 μl 80% methanol followed by centrifugation at 4°C for 15 min at 20,000 × *g*; supernatants were dried in a vacuum centrifuge. 25 μl of a 2% methoxyamine hydrochloride solution (20 mg dissolved in 1 ml pyridine) was added to the dried fractions, which were then incubated at 37°C for 90 min. Then, 75 μl of N-tert-butyldimethylsilyl-N-methyltrifluoroacetamide with 1% N-tert-butyldimethyl-chlorosilane (Sigma-Aldrich) was added and the reaction was carried out for 30 min at 60°C. Reaction mixtures were centrifuged for 15 min at 20,000 × *g* at 4°C in order to remove insolubilities, the supernatant was transferred to a glass vial with conical insert (Agilent). GC-MS analyses were performed on an Agilent 7890A GC equipped with a HP-5 ms 5% Phenyl Methyl Silox (30 m–0.25 mm i.d. – 0.25 μm; Agilent Technologies) capillary column, interfaced with a triple quadrupole tandem mass spectrometer (Agilent 7000B, Agilent Technologies) operating under ionization by electron impact at 70 eV. The injection port, interface and ion source temperatures were kept at 230°C. Temperature of the quadrupoles was kept at 150°C. The injection

volume was 1 μl, and samples were injected at 1:10 split ratio. Helium flow was kept constant at 1 ml/min. The temperature of the column started at 100°C for 5 min and increased to 260°C at 2°C/min. Next, a 40°C/min gradient was carried out until temp reached 300°C. After the gradient, the column was heated for another 3 min at 325°C. The GC-MS analyses were performed in Selected Ion Monitoring (SIM) scanning for the isotopic pattern of metabolites.

Ex vivo models

Aortic ring relaxation

Vasomotor function was assessed in segments of thoracic aorta as previously described (Viswambharan *et al*, 2017). Segments were mounted in an organ bath (Panlab; ADInstruments Ltd., UK) containing Krebs Henseleit buffer and equilibrated at a resting tension of 3 g for 2 h in the presence of CB-839 (1 μM) or vehicle control. Relaxation responses to cumulative addition of acetylcholine (1 nM–10 μM) and then sodium nitroprusside (0.1 nM–1 μM) were performed after pre-constriction with phenylephrine (300 nM), and responses were expressed as percentage decrement in pre-constricted tension.

In vivo models

GLS1^{ECKO} mice

To obtain inducible EC-specific GLS1 knockout mice, GLS1$^{lox/lox}$ mice (Mingote *et al*, 2015) were intercrossed with Pdgfb-Cre^{ERT2} mice (Claxton *et al*, 2008). *Neonatal retinal angiogenesis*: EC-specific GLS1 deletion was achieved by intraperitoneal (i.p.) administration of tamoxifen (Sigma; 10 mg/kg; dissolved in 1:10 EtOH:oil solution) once at P2. At P5, pups were euthanized, eyes were enucleated, fixed with 2% PFA for 2 h. Isolectin-B4 (IB4), phH3, and NG2 stainings were performed as previously described (Pitulescu *et al*, 2010; De Bock *et al*, 2013b; Schoors *et al*, 2015). Radial outgrowth, branching points, number of distal sprouts, pericyte coverage (NG2$^+$ area), and phH3$^+$ cell numbers per vessel area were analyzed using the NIH ImageJ software package and the Leica MM AF morphometric analysis software (Carl Zeiss, Munich, Germany) with in-house-developed journals. *Oxygen-induced retinopathy*: Oxygen-induced retinopathy (ROP; Scott & Fruttiger, 2010) was induced by exposing C57BL/6 pups to 70% oxygen from P7 to P12. At P13, pups were placed back in normoxia and injected daily with 40 mg/kg CB-839 or vehicle. At P17, pups were euthanized and eyes were enucleated, fixed in 4% PFA and retinal flat mounts were stained with isolectin-B4 as described (De Bock *et al*, 2013b; Schoors *et al*, 2015). Mosaic images were captured using the inverted Leica DMI6000B epifluorescence microscope (Leica, Manheim, Germany), and analysis of the vascular tuft area was performed with NIH ImageJ software. *Asparaginase treatment*: Newborn pups were IP-injected with 2 U/g/day asparaginase for 4 consecutive days (P1–P4). Retinas were isolated at P4 as described above. Prior randomization was not applicable for any of the above mouse models given that all animal treatments were done in baseline conditions. No statistical methods were used to predetermine the sample size. For all mouse experiments, data analysis was done by experimenters blinded to the group allocation. All animal procedures were approved by the Institutional Animal Care and Research Advisory Committee of the University of Leuven.

Statistics

Data represent mean ± SEM of pooled experiments, while "n" values represent the number of independent experiments performed or the number of individual mice phenotyped. All experiments with freshly isolated ECs were performed at least three times using different donors. Statistical significance between groups was calculated with two-tailed unpaired t-test. Sample size for each experiment was not pre-determined. For Fig 1A, a one-sample t-test versus a hypothetical value of 0 was used; for Fig 2S and X, the same test was used versus a hypothetical value of 1. An area under the curve (AUC) analysis was used in Fig 2T and U. All statistical analyses were performed with GraphPad Prism. A $P < 0.05$ was considered significant.

Expanded View for this article is available online.

Author contributions

HH, GE, SV, AZ, UB, BC, AV, NY, JK, LB, RC, JG, KB, SW, BG, LS, SV, and MD performed experiments and/or analyzed data; SR provided materials; HH, GE, SV, and PC designed the experiments; HH, GE, SV, and PC wrote the paper; HH, GE, JG, BG, and PC conceptualized the metabolic analysis; PC conceived and directed the study. All authors discussed the results and commented on the manuscript.

Conflict of interest

The authors declare that they have no conflict of interest.

References

Ahlman B, Andersson K, Leijonmarck CE, Ljungqvist O, Hedenborg L, Wernerman J (1994) Short-term starvation alters the free amino acid content of the human intestinal mucosa. *Clin Sci (Lond)* 86: 653–662

Ameri K, Luong R, Zhang H, Powell AA, Montgomery KD, Espinosa I, Bouley DM, Harris AL, Jeffrey SS (2010) Circulating tumour cells demonstrate an altered response to hypoxia and an aggressive phenotype. *Br J Cancer* 102: 561–569

Armstrong MD, Stave U (1973) A study of plasma free amino acid levels. II. Normal values for children and adults. *Metabolism* 22: 561–569

Aslanian AM, Fletcher BS, Kilberg MS (2001) Asparagine synthetase expression alone is sufficient to induce l-asparaginase resistance in MOLT-4 human leukaemia cells. *Biochem J* 357: 321–328

Balasubramanian MN, Butterworth EA, Kilberg MS (2013) Asparagine synthetase: regulation by cell stress and involvement in tumor biology. *Am J Physiol Endocrinol Metab* 304: E789–E799

Ben-Sahra I, Howell JJ, Asara JM, Manning BD (2013) Stimulation of *de novo* pyrimidine synthesis by growth signaling through mTOR and S6K1. *Science* 339: 1323–1328

Bentley K, Mariggi G, Gerhardt H, Bates PA (2009) Tipping the balance: robustness of tip cell selection, migration and fusion in angiogenesis. *PLoS Comput Biol* 5: e1000549

Burt ME, Aoki TT, Gorschboth CM, Brennan MF (1983) Peripheral tissue metabolism in cancer-bearing man. *Ann Surg* 198: 685–691

Carlotti F, Bazuine M, Kekarainen T, Seppen J, Pognonec P, Maassen JA, Hoeben RC (2004) Lentiviral vectors efficiently transduce quiescent mature 3T3-L1 adipocytes. *Mol Ther* 9: 209–217

Chan WK, Lorenzi PL, Anishkin A, Purwaha P, Rogers DM, Sukharev S, Rempe SB, Weinstein JN (2014) The glutaminase activity of L-asparaginase is not required for anticancer activity against ASNS-negative cells. *Blood* 123: 3596–3606

Claxton S, Kostourou V, Jadeja S, Chambon P, Hodivala-Dilke K, Fruttiger M (2008) Efficient, inducible Cre-recombinase activation in vascular endothelium. *Genesis* 46: 74–80

Cui H, Darmanin S, Natsuisaka M, Kondo T, Asaka M, Shindoh M, Higashino F, Hamuro J, Okada F, Kobayashi M, Nakagawa K, Koide H, Kobayashi M (2007) Enhanced expression of asparagine synthetase under glucose-deprived conditions protects pancreatic cancer cells from apoptosis induced by glucose deprivation and cisplatin. *Cancer Res* 67: 3345–3355

De Bock K, Georgiadou M, Carmeliet P (2013a) Role of endothelial cell metabolism in vessel sprouting. *Cell Metab* 18: 634–647

De Bock K, Georgiadou M, Schoors S, Kuchnio A, Wong BW, Cantelmo AR, Quaegebeur A, Ghesquiere B, Cauwenberghs S, Eelen G, Phng LK, Betz I, Tembuyser B, Brepoels K, Welti J, Geudens I, Segura I, Cruys B, Bifari F, Decimo I *et al* (2013b) Role of PFKFB3-driven glycolysis in vessel sprouting. *Cell* 154: 651–663

DeBerardinis RJ, Mancuso A, Daikhin E, Nissim I, Yudkoff M, Wehrli S, Thompson CB (2007) Beyond aerobic glycolysis: transformed cells can engage in glutamine metabolism that exceeds the requirement for protein and nucleotide synthesis. *Proc Natl Acad Sci USA* 104: 19345–19350

DeBerardinis RJ, Cheng T (2010) Q's next: the diverse functions of glutamine in metabolism, cell biology and cancer. *Oncogene* 29: 313–324

Duran RV, Oppliger W, Robitaille AM, Heiserich L, Skendaj R, Gottlieb E, Hall MN (2012) Glutaminolysis activates Rag-mTORC1 signaling. *Mol Cell* 47: 349–358

Eelen G, de Zeeuw P, Simons M, Carmeliet P (2015) Endothelial cell metabolism in normal and diseased vasculature. *Circ Res* 116: 1231–1244

Fendt SM, Bell EL, Keibler MA, Olenchock BA, Mayers JR, Wasylenko TM, Vokes NI, Guarente L, Vander Heiden MG, Stephanopoulos G (2013) Reductive glutamine metabolism is a function of the alpha-ketoglutarate to citrate ratio in cells. *Nat Commun* 4: 2236

Fernandez CA, Des Rosiers C, Previs SF, David F, Brunengraber H (1996) Correction of 13C mass isotopomer distributions for natural stable isotope abundance. *J Mass Spectrom* 31: 255–262

Forstermann U, Sessa WC (2012) Nitric oxide synthases: regulation and function. *Eur Heart J* 33: 829–837, 837a–837d

Geudens I, Gerhardt H (2011) Coordinating cell behaviour during blood vessel formation. *Development* 138: 4569–4583

Gong SS, Basilico C (1990) A mammalian temperature-sensitive mutation affecting G1 progression results from a single amino acid substitution in asparagine synthetase. *Nucleic Acids Res* 18: 3509–3513

Gross MI, Demo SD, Dennison JB, Chen L, Chernov-Rogan T, Goyal B, Janes JR, Laidig GJ, Lewis ER, Li J, Mackinnon AL, Parlati F, Rodriguez ML, Shwonek PJ, Sjogren EB, Stanton TF, Wang T, Yang J, Zhao F, Bennett MK (2014) Antitumor activity of the glutaminase inhibitor CB-839 in triple-negative breast cancer. *Mol Cancer Ther* 13: 890–901

Han T, Kang D, Ji D, Wang X, Zhan W, Fu M, Xin HB, Wang JB (2013) How does cancer cell metabolism affect tumor migration and invasion? *Cell Adh Migr* 7: 395–403

Han T, Guo M, Zhang T, Gan M, Xie C, Wang JB (2017) A novel glutaminase inhibitor-968 inhibits the migration and proliferation of non-small cell lung cancer cells by targeting EGFR/ERK signaling pathway. *Oncotarget* 8: 28063–28073

Harding HP, Zhang Y, Zeng H, Novoa I, Lu PD, Calfon M, Sadri N, Yun C, Popko B, Paules R, Stojdl DF, Bell JC, Hettmann T, Leiden JM, Ron D (2003) An integrated stress response regulates amino acid metabolism and resistance to oxidative stress. *Mol Cell* 11: 619–633

van den Heuvel AP, Jing J, Wooster RF, Bachman KE (2012) Analysis of glutamine dependency in non-small cell lung cancer: GLS1 splice variant GAC is essential for cancer cell growth. *Cancer Biol Ther* 13: 1185–1194

Hosios AM, Hecht VC, Danai LV, Johnson MO, Rathmell JC, Steinhauser ML, Manalis SR, Vander Heiden MG (2016) Amino acids rather than glucose account for the majority of cell mass in proliferating mammalian cells. *Dev Cell* 36: 540–549

Hou YC, Wu JM, Wang MY, Wu MH, Chen KY, Yeh SL, Lin MT (2014) Glutamine supplementation attenuates expressions of adhesion molecules and chemokine receptors on T cells in a murine model of acute colitis. *Mediators Inflamm* 2014: 837107

Jaffe EA, Nachman RL, Becker CG, Minick CR (1973) Culture of human endothelial cells derived from umbilical veins. Identification by morphologic and immunologic criteria. *J Clin Investig* 52: 2745–2756

Jakobsson L, Franco CA, Bentley K, Collins RT, Ponsioen B, Aspalter IM, Rosewell I, Busse M, Thurston G, Medvinsky A, Schulte-Merker S, Gerhardt H (2010) Endothelial cells dynamically compete for the tip cell position during angiogenic sprouting. *Nat Cell Biol* 12: 943–953

Jewell JL, Russell RC, Guan KL (2013) Amino acid signalling upstream of mTOR. *Nat Rev Mol Cell Biol* 14: 133–139

Jewell JL, Kim YC, Russell RC, Yu FX, Park HW, Plouffe SW, Tagliabracci VS, Guan KL (2015) Metabolism. Differential regulation of mTORC1 by leucine and glutamine. *Science* 347: 194–198

Jousse C, Averous J, Bruhat A, Carraro V, Mordier S, Fafournoux P (2004) Amino acids as regulators of gene expression: molecular mechanisms. *Biochem Biophys Res Commun* 313: 447–452

Kalucka J, Bierhansl L, Wielockx B, Carmeliet P, Eelen G (2017) Interaction of endothelial cells with macrophages-linking molecular and metabolic signaling. *Pflugers Arch* 469: 473–483

Kawedia JD, Rytting ME (2014) Asparaginase in acute lymphoblastic leukemia. *Clin Lymphoma Myeloma Leuk* 14(Suppl): S14–S17

Kilberg MS, Barbosa-Tessmann IP (2002) Genomic sequences necessary for transcriptional activation by amino acid deprivation of mammalian cells. *J Nutr* 132: 1801–1804

Kim DS, Jue SS, Lee SY, Kim YS, Shin SY, Kim EC (2014) Effects of glutamine on proliferation, migration, and differentiation of human dental pulp cells. *J Endod* 40: 1087–1094

Kim B, Li J, Jang C, Arany Z (2017) Glutamine fuels proliferation but not migration of endothelial cells. *EMBO J* 36: 2321–2333

Korff T, Krauss T, Augustin HG (2004) Three-dimensional spheroidal culture of cytotrophoblast cells mimics the phenotype and differentiation of cytotrophoblasts from normal and preeclamptic pregnancies. *Exp Cell Res* 297: 415–423

Krall AS, Xu S, Graeber TG, Braas D, Christofk HR (2016) Asparagine promotes cancer cell proliferation through use as an amino acid exchange factor. *Nat Commun* 7: 11457

Kume T (2010) Specification of arterial, venous, and lymphatic endothelial cells during embryonic development. *Histol Histopathol* 25: 637–646

Laplante M, Sabatini DM (2009) An emerging role of mTOR in lipid biosynthesis. *Curr Biol* 19: R1046–R1052

Leighton B, Curi R, Hussein A, Newsholme EA (1987) Maximum activities of some key enzymes of glycolysis, glutaminolysis, Krebs cycle and fatty acid utilization in bovine pulmonary endothelial cells. *FEBS Lett* 225: 93–96

Li J, Song P, Zhu L, Aziz N, Zhou Q, Zhang Y, Xu W, Feng L, Chen D, Wang X, Jin H (2017) Synthetic lethality of glutaminolysis inhibition, autophagy inactivation and asparagine depletion in colon cancer. *Oncotarget* 8: 42664–42672

Liu S, Premont RT, Kontos CD, Huang J, Rockey DC (2003) Endothelin-1 activates endothelial cell nitric-oxide synthase via heterotrimeric G-protein betagamma subunit signaling to protein jinase B/Akt. *J Biol Chem* 278: 49929–49935

Lohmann R, Souba WW, Bode BP (1999) Rat liver endothelial cell glutamine transporter and glutaminase expression contrast with parenchymal cells. *Am J Physiol* 276: G743–G750

Mashimo T, Pichumani K, Vemireddy V, Hatanpaa KJ, Singh DK, Sirasanagandla S, Nannepaga S, Piccirillo SG, Kovacs Z, Foong C, Huang Z, Barnett S, Mickey BE, DeBerardinis RJ, Tu BP, Maher EA, Bachoo RM (2014) Acetate is a bioenergetic substrate for human glioblastoma and brain metastases. *Cell* 159: 1603–1614

Metallo CM, Gameiro PA, Bell EL, Mattaini KR, Yang J, Hiller K, Jewell CM, Johnson ZR, Irvine DJ, Guarente L, Kelleher JK, Vander Heiden MG, Iliopoulos O, Stephanopoulos G (2012) Reductive glutamine metabolism by IDH1 mediates lipogenesis under hypoxia. *Nature* 481: 380–384

Michieli P, Mazzone M, Basilico C, Cavassa S, Sottile A, Naldini L, Comoglio PM (2004) Targeting the tumor and its microenvironment by a dual-function decoy Met receptor. *Cancer Cell* 6: 61–73

Mingote S, Masson J, Gellman C, Thomsen GM, Lin CS, Merker RJ, Gaisler-Salomon I, Wang Y, Ernst R, Hen R, Rayport S (2015) Genetic pharmacotherapy as an early CNS drug development strategy: testing glutaminase inhibition for schizophrenia treatment in adult mice. *Front Syst Neurosci* 9: 165

Mullen AR, Wheaton WW, Jin ES, Chen PH, Sullivan LB, Cheng T, Yang Y, Linehan WM, Chandel NS, DeBerardinis RJ (2012) Reductive carboxylation supports growth in tumour cells with defective mitochondria. *Nature* 481: 385–388

Newburg DS, Frankel DL, Fillios LC (1975) An asparagine requirement in young rats fed the dietary combinations of aspartic acid, glutamine, and glutamic acid. *J Nutr* 105: 356–363

Pan Y, Chen H, Siu F, Kilberg MS (2003) Amino acid deprivation and endoplasmic reticulum stress induce expression of multiple activating transcription factor-3 mRNA species that, when overexpressed in HepG2 cells, modulate transcription by the human asparagine synthetase promoter. *J Biol Chem* 278: 38402–38412

Parri M, Chiarugi P (2013) Redox molecular machines involved in tumor progression. *Antioxid Redox Signal* 19: 1828–1845

Parsa AT, Waldron JS, Panner A, Crane CA, Parney IF, Barry JJ, Cachola KE, Murray JC, Tihan T, Jensen MC, Mischel PS, Stokoe D, Pieper RO (2007) Loss of tumor suppressor PTEN function increases B7-H1 expression and immunoresistance in glioma. *Nat Med* 13: 84–88

dela Paz NG, D'Amore PA (2009) Arterial versus venous endothelial cells. *Cell Tissue Res* 335: 5–16.

Pieters R, Hunger SP, Boos J, Rizzari C, Silverman L, Baruchel A, Goekbuget N, Schrappe M, Pui CH (2011) L-asparaginase treatment in acute lymphoblastic leukemia: a focus on Erwinia asparaginase. *Cancer* 117: 238–249

Pitulescu ME, Schmidt I, Benedito R, Adams RH (2010) Inducible gene targeting in the neonatal vasculature and analysis of retinal angiogenesis in mice. *Nat Protoc* 5: 1518–1534

Potente M, Gerhardt H, Carmeliet P (2011) Basic and therapeutic aspects of angiogenesis. *Cell* 146: 873–887

Qie S, Liang D, Yin C, Gu W, Meng M, Wang C, Sang N (2012) Glutamine depletion and glucose depletion trigger growth inhibition via distinctive gene expression reprogramming. *Cell Cycle* 11: 3679–3690

Richards NG, Kilberg MS (2006) Asparagine synthetase chemotherapy. *Annu Rev Biochem* 75: 629–654

Rodrigues MF, Obre E, de Melo FH, Santos GC Jr, Galina A, Jasiulionis MG, Rossignol R, Rumjanek FD, Amoedo ND (2016) Enhanced OXPHOS, glutaminolysis and beta-oxidation constitute the metastatic phenotype of melanoma cells. *Biochem J* 473: 703–715

Sakai T, Jung HS, Sato O, Yamada MD, You DJ, Ikebe R, Ikebe M (2015) Structure and regulation of the movement of human myosin VIIA. *J Biol Chem* 290: 17587–17598

Schoors S, De Bock K, Cantelmo AR, Georgiadou M, Ghesquiere B, Cauwenberghs S, Kuchnio A, Wong BW, Quaegebeur A, Goveia J, Bifari F, Wang X, Blanco R, Tembuyser B, Cornelissen I, Bouche A, Vinckier S, Diaz-Moralli S, Gerhardt H, Telang S *et al* (2014) Partial and transient reduction of glycolysis by PFKFB3 blockade reduces pathological angiogenesis. *Cell Metab* 19: 37–48

Schoors S, Bruning U, Missiaen R, Queiroz KC, Borgers G, Elia I, Zecchin A, Cantelmo AR, Christen S, Goveia J, Heggermont W, Godde L, Vinckier S, Van Veldhoven PP, Eelen G, Schoonjans L, Gerhardt H, Dewerchin M, Baes M, De Bock K *et al* (2015) Fatty acid carbon is essential for dNTP synthesis in endothelial cells. *Nature* 520: 192–197

Schug ZT, Peck B, Jones DT, Zhang Q, Grosskurth S, Alam IS, Goodwin LM, Smethurst E, Mason S, Blyth K, McGarry L, James D, Shanks E, Kalna G, Saunders RE, Jiang M, Howell M, Lassailly F, Thin MZ, Spencer-Dene B *et al* (2015) Acetyl-CoA synthetase 2 promotes acetate utilization and maintains cancer cell growth under metabolic stress. *Cancer Cell* 27: 57–71

Scioscia KA, Snyderman CH, Wagner R (1998) Altered serum amino acid profiles in head and neck cancer. *Nutr Cancer* 30: 144–147

Scott A, Fruttiger M (2010) Oxygen-induced retinopathy: a model for vascular pathology in the retina. *Eye (Lond)* 24: 416–421

Scriver CR, Gregory DM, Sovetts D, Tissenbaum G (1985) Normal plasma free amino acid values in adults: the influence of some common physiological variables. *Metabolism* 34: 868–873

Semba RD, Shardell M, Sakr Ashour FA, Moaddel R, Trehan I, Maleta KM, Ordiz MI, Kraemer K, Khadeer MA, Ferrucci L, Manary MJ (2016) Child stunting is associated with low circulating essential amino acids. *EBioMedicine* 6: 246–252

Son J, Lyssiotis CA, Ying H, Wang X, Hua S, Ligorio M, Perera RM, Ferrone CR, Mullarky E, Shyh-Chang N, Kang Y, Fleming JB, Bardeesy N, Asara JM, Haigis MC, DePinho RA, Cantley LC, Kimmelman AC (2013) Glutamine supports pancreatic cancer growth through a KRAS-regulated metabolic pathway. *Nature* 496: 101–105

Stahl A, Connor KM, Sapieha P, Chen J, Dennison RJ, Krah NM, Seaward MR, Willett KL, Aderman CM, Guerin KI, Hua J, Lofqvist C, Hellstrom A, Smith LE (2010) The mouse retina as an angiogenesis model. *Invest Ophthalmol Vis Sci* 51: 2813–2826

Suliman ME, Qureshi AR, Stenvinkel P, Pecoits-Filho R, Barany P, Heimburger O, Anderstam B, Rodriguez Ayala E, Divino Filho JC, Alvestrand A, Lindholm B (2005) Inflammation contributes to low plasma amino acid concentrations in patients with chronic kidney disease. *Am J Clin Nutr* 82: 342–349

Tardito S, Oudin A, Ahmed SU, Fack F, Keunen O, Zheng L, Miletic H, Sakariassen PO, Weinstock A, Wagner A, Lindsay SL, Hock AK, Barnett SC, Ruppin E, Morkve SH, Lund-Johansen M, Chalmers AJ, Bjerkvig R, Niclou SP, Gottlieb E (2015) Glutamine synthetase activity fuels nucleotide biosynthesis and supports growth of glutamine-restricted glioblastoma. *Nat Cell Biol* 17: 1556–1568

Tong WH, Pieters R, Kaspers GJ, te Loo DM, Bierings MB, van den Bos C, Kollen WJ, Hop WC, Lanvers-Kaminsky C, Relling MV, Tissing WJ, van der Sluis IM (2014) A prospective study on drug monitoring of PEGasparaginase and Erwinia asparaginase and asparaginase antibodies in pediatric acute lymphoblastic leukemia. *Blood* 123: 2026–2033

Ubuka T, Meister A (1971) Studies on the utilization of asparagine by mouse leukemia cells. *J Natl Cancer Inst* 46: 291–298

Unterluggauer H, Mazurek S, Lener B, Hutter E, Eigenbrodt E, Zwerschke W, Jansen-Durr P (2008) Premature senescence of human endothelial cells induced by inhibition of glutaminase. *Biogerontology* 9: 247–259

Viswambharan H, Yuldasheva NY, Sengupta A, Imrie H, Gage MC, Haywood N, Walker AM, Skromna A, Makova N, Galloway S, Shah P, Sukumar P, Porter KE, Grant PJ, Shah AM, Santos CX, Li J, Beech DJ, Wheatcroft SB, Cubbon RM *et al* (2017) Selective enhancement of insulin sensitivity in the endothelium *in vivo* reveals a novel proatherosclerotic signaling loop. *Circ Res* 120: 784–798

Wise DR, Thompson CB (2010) Glutamine addiction: a new therapeutic target in cancer. *Trends Biochem Sci* 35: 427–433

Wu G, Haynes TE, Li H, Meininger CJ (2000) Glutamine metabolism in endothelial cells: ornithine synthesis from glutamine via pyrroline-5-carboxylate synthase. *Comp Biochem Physiol A Mol Integr Physiol* 126: 115–123

Zhang J, Fan J, Venneti S, Cross JR, Takagi T, Bhinder B, Djaballah H, Kanai M, Cheng EH, Judkins AR, Pawel B, Baggs J, Cherry S, Rabinowitz JD, Thompson CB (2014) Asparagine plays a critical role in regulating cellular adaptation to glutamine depletion. *Mol Cell* 56: 205–218

Zhang B, Fan J, Zhang X, Shen W, Cao Z, Yang P, Xu Z, Ju D (2016) Targeting asparagine and autophagy for pulmonary adenocarcinoma therapy. *Appl Microbiol Biotechnol* 100: 9145–9161

Zhang J, Pavlova NN, Thompson CB (2017) Cancer cell metabolism: the essential role of the nonessential amino acid, glutamine. *EMBO J* 36: 1302–1315